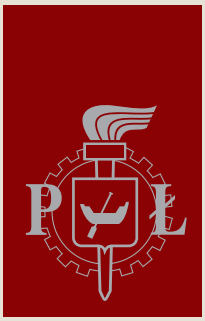

Lodz University of Technology

SCIENTIFIC BULLETIN

PHYSICS

Vol. 35

LODZ 2014

LODZ UNIVERSITY OF TECHNOLOGY

SCIENTIFIC BULLETIN
No. 1192

PHYSICS
Vol. 35

LODZ 2014

ZESZYTY NAUKOWE POLITECHNIKI ŁÓDZKIEJ

SCIENTIFIC BULLETIN OF THE LODZ UNIVERSITY OF TECHNOLOGY

BULLETIN SCIENTIFIQUE
DE L'UNIVERSITÉ POLYTECHNIQUE DE LODZ

НАУЧНЫЕ ЗАПИСКИ
ЛОДЗИНСКОГО ПОЛИТЕХНИЧЕСКОГО УНИВЕРСИТЕТА

WISSENSCHAFTLICHE HEFTE
DER TECHNISCHEN UNIVERSITÄT IN LODZ

Editor of series: **Assoc. Professor Grzegorz Derfel, Ph.D., D.Sc.**

Subject Editor of series: **Assoc. Professor Jolanta Prywer, Ph.D., D.Sc.**

Secretary of series: **Marek Wojciechowski, Ph.D.**

Printed version of the journal is the main version

Adres Redakcji – Адрес Редакции – Editor's Office
Adresse de Redaction – Schriftleitungsadresse:

WYDAWNICTWO POLITECHNIKI ŁÓDZKIEJ
90-924 Łódź, ul. Wólczańska 223
tel. 42-631-20-87, fax 42-631-25-38
e-mail: zamowienia@info.p.lodz.pl
www.wydawnictwa.p.lodz.pl

ISSN 1505-1013

Nakład 100 egz. Ark. druk. 5,0. Papier offset. 80 g 70 x 100
Druk ukończono w lutym 2015 r.
Wykonano w Drukarni Offsetowej Quick-Druk, 90-562 Łódź, ul. Łąkowa

CONTENTS

SCIENTIFIC BULLETIN OF THE LODZ UNIVERSITY OF TECHNOLOGY
No. 1192 Physics, Vol. 35 2014

MAREK IZDEBSKI, RAFAŁ LEDZION

Institute of Physics, Lodz University of Technology
ul. Wólczańska 219,90-924 Łódź, Poland, e-mail: izdebski@p.lodz.pl

MODULATION TECHNIQUE USED FOR MEASUREMENT OF VERY WEAK LINEAR BIREFRINGENCE AND DICHROISM IN LIQUIDS ON THE EXAMPLE OF CASTOR OIL BETWEEN METAL ELECTRODES

A technique for measurement of very weak linear birefringence of the order of 10^{-7} and dichroism in liquids is proposed. The method is based on the polarimetric technique. A characteristic feature is that the experimental setup enables the measurement of linear birefringence combined with electro-optic effect as well as the measurement of dichroism combined with electro-optic effect. The combination of the effect which does not show rapid changes with the effect which depends on alternating electric field allows to improve the sensitivity of the method (in comparison to the earlier static method). This was achieved by use of lock-in amplifier that measures only the selected harmonic with very high selectivity. The theoretical considerations are illustrated by the results of measurements for castor oil.

Keywords: castor oil, optical polarimetric technique, linear birefringence, dichroism, electro-optic effect.

1. INTRODUCTION

Castor oil is known for its natural optical activity, thus its internal symmetry can be described only by those Curie groups which allow for this effect, namely $\infty\infty$, $\infty 2$, and ∞. Our previous studies have shown that castor oil placed between two plane-parallel metal plates exhibits dichroism and linear birefringence of the order of 10^{-7} with the optical axis directed perpendicularly to the electrodes, which limits the possible symmetries to the $\infty 2$ and ∞ groups [1]. Moreover, our recent measurements have shown that the quadratic

electro-optic and quadratic elecrogyration effect (optical activity induced by electric field) manifest themselves in castor oil, while the linear effect is not clearly observed, which indicates the $\infty 2$ symmetry [2].

The aim of this work is to propose a method for measuring very weak linear birefringence and dichroism, which should be more sensitive than the method proposed earlier in Ref. [1]. Moreover, the method should be more suitable for automation than the previous one, which required multiple search of polarizers orientations corresponding to the minimum and maximum of light transmission through the measurement system. Our main motivation to develop better measurement method involves quality control of vegetable oils of industrial importance.

Early attempts to apply optical constants for assessing the quality of vegetable oils focused mainly on refractive index and a rotation of the plane of polarization. Testing of these constants may be used as a simple method for detecting serious adulteration of castor oil with cheaper oil [3]. However, our observations show a rather poor suitability of the method due to its to low sensitivity, e.g., to study the effect of oxidation of the oil. The optical constants, which seem to be more promising, are:

- Kerr constant (describing quadratic electro-optic effect) which shows a clear relationship with aging process in castor oil [4],
- Verdet constant (describing the effect of optical activity induced by an applied magnetic field), which can be used in authentication techniques of olive oil and probably also other vegetable oils [5],
- the linear birefringence and dichroism; our preliminary observations indicate that they may be the next optical effects useful to indicate changes in the oils quality.

Liquids with very weak linear birefringence of the order of 10^{-7} are also interesting from a cognitive point of view, as a case of liquids exhibiting a slight orientational ordering of molecules, which essentially distinguishes them from the isotropic liquid as well as liquid crystals.

2. THEORETICAL ANALYSIS

2.1. Impermeability tensor

The real part of electric impermeability tensor [B] at optical frequencies for non-absorbing medium of the $\infty 2$ symmetry written in the principal axes system XYZ (where the Z axis is the optical axis) with the accuracy to the terms proportional to the square of applied electric field E is as follows:

$$\mathrm{Re}[B]=\begin{bmatrix} n_{01}^{-2}+q_{13}E^2 & 0 & 0 \\ 0 & n_{01}^{-2}+q_{13}E^2 & 0 \\ 0 & 0 & n_{03}^{-2}+q_{33}E^2 \end{bmatrix}, \tag{1}$$

where n_{01} and n_{03} are the major field-free refractive indices and q_{ij} are the components of the quadratic electro-optic tensors. Due to the observed dependence of the optical axis in castor oil on the orientation of the electrodes (see Ref. 1) we have assumed in equations (1) and (4), that the only possible form of the electric field vector written in the *XYZ* coordinates is **E** = (0, 0, *E*). Although the linear electro-optic effect is not forbidden by the ∞2 symmetry, it may not manifest itself for this particular field direction. The forms of the tensors describing the natural linear birefringence, natural optical activity, linear and quadratic electro-optic effect, and linear and quadratic electrogyration effect can be found, e.g., in Refs. [2,6,7].

The natural and electric field induced optical activity is traditionally described by the imaginary antisymmetric part of the relative permittivity tensor [*K*] at optical frequencies [8]:

$$\mathrm{Im}[K]=\begin{bmatrix} 0 & -G_3 & G_2 \\ G_3 & 0 & -G_1 \\ -G_2 & G_1 & 0 \end{bmatrix}, \tag{2}$$

where G_1, G_2 and G_3 are the elements of the gyration vector **G** for a given wave propagation vector **s**:

$$\mathbf{G} = [g]\mathbf{s}. \tag{3}$$

In Eq. (3) [*g*] is a second rank gyration axial tensor described by a real 3×3 matrix. In the case of liquids of the ∞2 symmetry and the field **E** = (0, 0, *E*) the tensor has the form:

$$[g]=\begin{bmatrix} g_{11}^{(0)}+\beta_{13}E^2 & 0 & 0 \\ 0 & g_{11}^{(0)}+\beta_{13}E^2 & 0 \\ 0 & 0 & g_{33}^{(0)}+\beta_{33}E^2 \end{bmatrix}, \tag{4}$$

where $g_{ii}^{(0)}$ are the components of natural optical activity tensor and β_{ij} are the components of the quadratic electrogyration tensor. When the tensors Re[*B*] and Im[*K*] are already known, the imaginary part of the [*B*] tensor can be found using the formula [9]:

$$\mathrm{Im}[B] = -[B]\,\mathrm{Im}[K]\,[B] \approx -\,\mathrm{Re}[B]\,\mathrm{Im}[K]\,\mathrm{Re}[B]. \tag{5}$$

The formulas (1)-(5) allow to find the total complex hermitian impermeability tensor [B] for non-absorbing liquid of the $\infty 2$ symmetry. In the case of absorbing medium the symmetry $B'_{ij} = B'^{*}_{ji}$ is not exactly satisfied, however, the perturbation of the symmetry is negligible in a typical case $1/\kappa >> \lambda$, where κ [m^{-1}] is the absorption coefficient and λ [m] is the wavelength of light.

Let us consider the configuration $\mathbf{s} = [1, 0, 0]$ and $\mathbf{E} = [0, 0, E]$. The total complex impermeability tensor, found from equations (1)-(5) for this configuration and written in the *XYZ* coordinates with accuracy to the terms proportional to E^2, has the following form:

$$[B] = \begin{bmatrix} n_{01}^{-2} + q_{13}E^2 & 0 & 0 \\ 0 & n_{01}^{-2} + q_{13}E^2 & B_{23} \\ 0 & -B_{23} & n_{03}^{-2} + q_{33}E^2 \end{bmatrix}, \tag{6}$$

where:

$$B_{23} = \mathrm{i}\left[n_{01}^{-2} n_{03}^{-2}\left(g_{11}^{(0)} + \beta_{13}E^2\right) + g_{11}^{(0)}\left(n_{01}^{-2} q_{33} + n_{03}^{-2} q_{13}\right)E^2\right]. \tag{7}$$

The terms in Eq. (7) containing the products of $g_{11}^{(0)}$ (of the order of 10^{-7}) and q_{ij} are negligible and the term $n_{01}^{-2} n_{03}^{-2}$ is very close to n_0^{-4}, where $n_0 = (n_{01}+n_{03})/2$ is the average refractive index.

2.2. Transmission of the light beam through the measurement system

The state of a monochromatic light passing through a system of plane-parallel optical elements can be found using Jones calculus (see, e.g., [10]). In our calculations, we used one of the most general form of a Jones M-matrix derived by Ratajczyk & Ścierski [10,11], which describes the transmission of light beam through any dichroic homogeneous elliptically birefringent media. In order to express the terms occurring in the matrix directly by the components of complex hermitian impermeability tensor, an additional formulas were applied which have been recently found using the eigenvalue approach [12].

Let us consider the measurement system composed of an ideal linear polarizer of any orientation α_p, a cuvette with oil in the form of a rectangular parallelepiped, and an ideal linear analyzer of the orientation $\alpha_a = \alpha_p - 45°$ or $\alpha_a = \alpha_p + 45°$. The intensity of the light I passing though the system relative to the intensity I_p directly behind the polarizer is given by [2]:

$$\begin{aligned}\frac{I}{I_\mathrm{p}} &= \frac{T_\mathrm{f}^2+T_\mathrm{s}^2}{4}+\\ &+\frac{\sqrt{2}}{2}\sin(45^\circ \mp 2\alpha_\mathrm{p})\frac{T_\mathrm{s}^2-T_\mathrm{f}^2}{2}\frac{B'_{22}-B'_{11}}{\sqrt{(B'_{11}-B'_{22})^2+4B'_{12}B'^{*}_{12}}}+\\ &\mp\frac{1}{8}\sin(4\alpha_\mathrm{p})\frac{(B'_{11}-B'_{22})^2}{(B'_{11}-B'_{22})^2+4B'_{12}B'^{*}_{12}}\left(T_\mathrm{f}^2+T_\mathrm{s}^2-2T_\mathrm{f}T_\mathrm{s}\cos\Gamma\right)+\\ &\pm\frac{T_\mathrm{f}T_\mathrm{s}\,\mathrm{Im}[B'_{12}]}{\sqrt{(B'_{11}-B'_{22})^2+4B'_{12}B'^{*}_{12}}}\sin\Gamma,\end{aligned} \tag{8}$$

where the upper signs in the "$\mp$" and "$\pm$" symbols correspond to $\alpha_\mathrm{a} = \alpha_\mathrm{p} + 45°$ and the lower signs to $\alpha_\mathrm{a} = \alpha_\mathrm{p} - 45°$, and B'_{ij} are the components of impermeability tensor written in the *X'Y'Z'* coordinate system traditionally used in Jones calculus, where the $+Z'$ axis is along the light beam **s'** = [0, 0, 1] and the $+X'$ axis defines the reference zero azimuth, T_f and T_s are the amplitude transmission coefficients for the fast and slow waves propagating in the oil sample, respectively, and Γ is the phase difference between the slow and fast waves. In order to simplify the form of equation (8) we omitted all terms containing a real part $\mathrm{Re}[B'_{12}]$, which vanishes for the symmetry under consideration both in the *X'Y'Z'* and *XYZ* coordinates. Moreover, since the relation $B'_{11}+B'_{22} >> \sqrt{(B'_{11}-B'_{22})^2+4B'_{12}B'^{*}_{12}}$ is fulfilled and n_{01} and n_{03} have very similar values, we can calculate Γ as [2,7]:

$$\Gamma \approx \frac{2\sqrt{2}\,\pi L}{\lambda}\frac{\sqrt{(B'_{11}-B'_{22})^2+4B'_{12}B'^{*}_{12}}}{(B'_{11}+B'_{22})^{3/2}} \approx \frac{\pi L\, n_0^3}{\lambda}\sqrt{(B'_{11}-B'_{22})^2+4B'_{12}B'^{*}_{12}}\,, \tag{9}$$

where *L* is the light path length in the oil.

The matrix of transformation from the *XYZ* to *X'Y'Z'* coordinates can be chosen in many ways, for example:

$$[\mathbf{a}] = \begin{bmatrix} 0 & 0 & -1 \\ 0 & 1 & 0 \\ 1 & 0 & 0 \end{bmatrix} \tag{10}$$

and the selected components of the matrix $[B'] = [\mathbf{a}][B][\mathbf{a}]^\mathrm{T}$ written in the *X'Y'Z'* coordinates are:

$$B'_{22} - B'_{11} = n_{01}^{-2} - n_{03}^{-2} + (q_{13}-q_{33})E^2\,, \tag{11}$$

$$B'_{12} = B_{23} \approx \mathrm{i}\, n_0^{-4} g_{11}^{(0)} + \mathrm{i}\, n_0^{-4} \beta_{13} E^2 . \tag{12}$$

Reliable and precise measurement of the intensity I relative to I_p, as in Eq. (8), is rather difficult task, but we can easily measure the changes in the intensity $I(E)$ induced by the applied field with respect to the constant component of the same intensity, I. The results of such measurements, however, do not provide sufficient data to determine the values of the coefficients T_f and T_s. Thus, in order to reduce the number of unknowns in the formula (8) we will introduce an average transmission coefficient:

$$\overline{T} = (T_f + T_s)/2 , \tag{13}$$

and dichroism defined as:

$$D = (T_f - T_s)/\overline{T} . \tag{14}$$

Now the expressions in Eq. (8), which depend on the transmission coefficients, can be written in the following form:

$$T_f T_s = \overline{T}^2 \left(1 - 0.25 D^2\right), \tag{15}$$

$$T_f^2 + T_s^2 = 2\overline{T}^2 \left(1 + 0.25 D^2\right), \tag{16}$$

$$T_f^2 - T_s^2 = 2\overline{T}^2 D^2 , \tag{17}$$

$$T_f^2 + T_s^2 - 2T_f T_s \cos\Gamma = 2\overline{T}^2 \left[(1 - \cos\Gamma) + 0.25 D^2 (1 + \cos\Gamma)\right]. \tag{18}$$

Substituting Eqs. (15)-(18) into (8) we can see, that all constant as well as field-dependent components are proportional to $\overline{T}^2$ and the effect of light absorption on the modulation of the emerging light can be described by only one parameter D. The dichroism described in the literature is traditionally divided into linear and circular dichroism, but the dichroism defined in this work by Eq. (14) can be used to describe any elliptical medium.

3. EXPERIMENTAL

The sample of castor oil for research purposes by SIGMA-ALDRICH company, product number 259853 (www.sigmaaldrich.com), was poured into a glass cuvette and the stainless steel plane-parallel electrodes spaced d = 4.13 mm were immersed in the oil. The cuvette was then placed between two polarizers and illuminated with He-Ne laser Melles Griot 05-LHP-171 at a wavelength λ = 632.8 nm, and the light beam was directed parallel to the electrodes with a length of L = 9,899 cm. The transmitted light was measured by a photodiode Thor Labs PDA100A-EC, which provides a voltage U proportional to the intensity I of emerging light. The measurements were performed at room temperature 22°C employing sinusoidally modulated electric field and the modulation index:

$$m_{2\omega} = U_{2\omega}/U_0 \tag{19}$$

was also determined, where $U_{2\omega}$ is the rms voltage measured at the second harmonic of the modulating generator by EG&G DSP Lock-in amplifier, model 7265, and U_0 is the DC component of the U voltage measured by Keithley 2700 multimeter.

The modulation voltage U_m was increased gradually from 910 to 3070 V RMS and an average values of $m_{2\omega}/U_\mathrm{m}^2$ were fitted by least square method for each measurement series. The average values of $m_{2\omega}/U_\mathrm{m}^2$ were found as the function of the azimuth of the polarizer α_p, which was changed from 0 to 360° with 5° steps, while the azimuth of the analyzer was $\alpha_\mathrm{a} = \alpha_\mathrm{p} + 45°$. Three days later analogous measurements were performed for $\alpha_\mathrm{a} = \alpha_\mathrm{p} - 45°$.

Then, based on the experimental dependence of $m_{2\omega}/U_\mathrm{m}^2$ on α_p, the theoretical dependence was numerically fitted:

$$\frac{m_{2\omega}}{U_\mathrm{m}^2} = \frac{I_{2\omega}/I_\mathrm{p}}{I_0/I_\mathrm{p}} U_\mathrm{m}^{-2}, \tag{20}$$

where $I_{2\omega}/I_\mathrm{p}$ and I_0/I_p were calculated as the coefficients in the following Fourier series:

$$\frac{I}{I_\mathrm{p}} = \frac{I_0}{I_\mathrm{p}} + \frac{I_\omega}{I_\mathrm{p}} \sin(\omega t + \varphi_1) + \frac{I_{2\omega}}{I_\mathrm{p}} \sin(2\omega t + \varphi_2) + \ldots, \tag{21}$$

for I/I_p given by Eq. (8) with substituted Eqs. (9), (11)-(18).

4. RESULTS

A large number of constants in Eqs. (8), (9) and (11)-(18) causes that we need to know in advance some of the values. We have used $n_0 = 1.48$ [2] and the Kerr constant $K = 1.5 \cdot 10^{-14}$ mV^{-2} [13], which allowed to calculate the effective coefficient of the quadratic electro-optic effect $|q_{33} - q_{13}| = 2\lambda K/n_0^3 \approx 5.8 \cdot 10^{-21}$ m^{2}V^{-2}. The value $g_{11}^{(0)} = -2.0 \cdot 10^{-7}$ was calculated on the basis of our measured optical rotation $\phi/L = -3.8°$/dm in the oil for $\lambda = 632.8$ nm and $\alpha_\mathrm{p} = 0$ using the relationship [2]:

$$g_{11}^{(0)} = \frac{\lambda n_0}{\pi} \frac{\phi}{L}. \tag{22}$$

The measured dependence of $m_{2\omega}/U_\mathrm{m}^2$ on α_p, obtained for the case $\alpha_\mathrm{a} = \alpha_\mathrm{p} - 45°$, is shown in Fig. 1, while the case $\alpha_\mathrm{a} = \alpha_\mathrm{p} + 45°$ is shown in Fig. 2. The combined effect of the linear birefringence with the quadratic electro-optic effect is related mainly to the component changing as $\pm\sin(4\alpha_\mathrm{p})$, while the combined

effect of the dichroism with the quadratic electro-optic effect gives mainly the result proportional to $\sin(45° \mp 2\alpha_p)$. With these data, we can provide unambiguous numerical fit of the absolute value of the linear birefringence:

$$|n_{03} - n_{01}| = (2.2 \pm 0.2)\cdot 10^{-7} \text{ (for the both series)}, \tag{23}$$

and absolute value of the dichroism:

$$|T_f - T_s| / \overline{T} = \begin{cases} (1.0 \pm 0.2)\cdot 10^{-2} \text{ for} \alpha_a = \alpha_p + 45^\circ, \\ (0.9 \pm 0.2)\cdot 10^{-2} \text{ for} \alpha_a = \alpha_p - 45^\circ. \end{cases} \tag{24}$$

Determining the positive or negative sign of $n_{03} - n_{01}$ and $T_f - T_s$ should be possible in future when the sign of $q_{33} - q_{13}$ will be known. Currently, we can determine only the signs of expressions involving two phenomena, namely:

$$(n_{03} - n_{01})(q_{33} - q_{13}) > 0, \tag{25}$$

$$(T_f - T_s)(q_{33} - q_{13}) < 0. \tag{26}$$

Our numerical studies have shown that for the field strengths smaller than 10^6 V/m rms, the values of the constants fitted numerically do not depend significantly on the field strength, but for larger strengths the $m_{2\omega}/U_m^2$ ratio cannot be considered as independent of U_m.

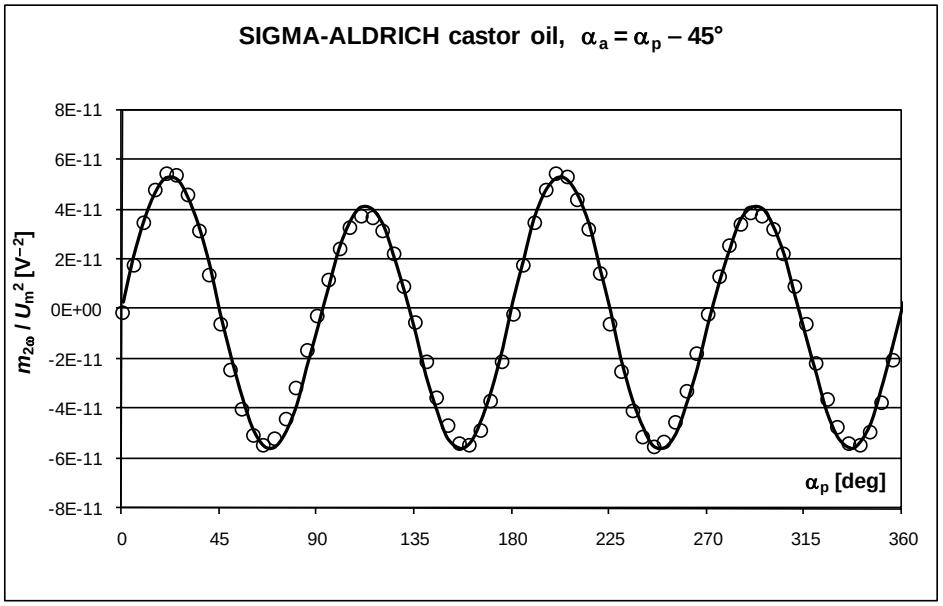

Fig. 1. The dependence of the ratio of modulation index $m_{2\omega}$ to the square of the modulation rms voltage U_m^2 on the polarizer azimuth α_p obtained for SIGMA-ALDRICH castor oil in the case $\alpha_a = \alpha_p - 45°$ and modulating field of frequency 417 Hz. Circles: the experimental data, curve: the interpolation fit

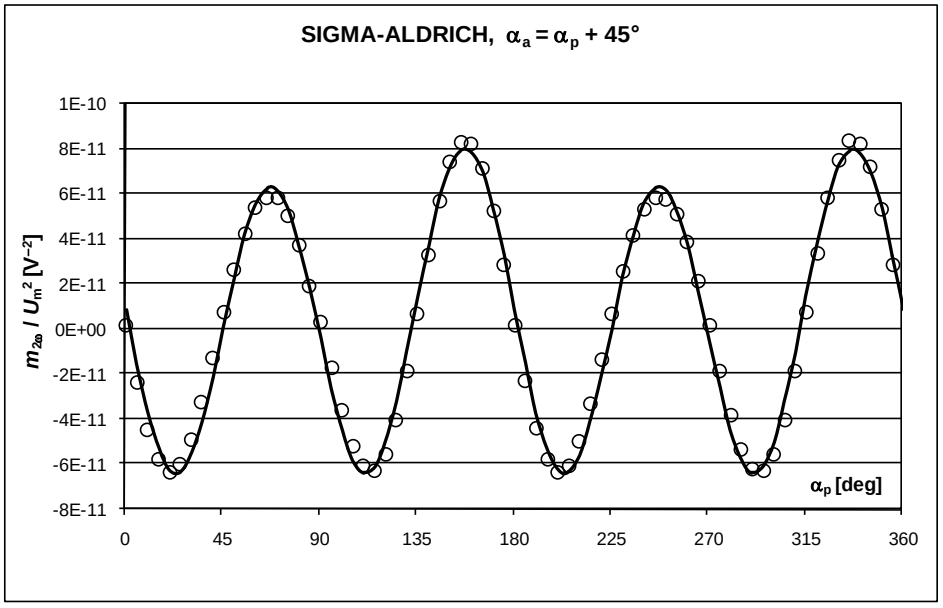

Fig. 2. The dependence of the ratio of modulation index $m_{2\omega}$ to the square of the modulation rms voltage U_m^2 on the polarizer azimuth α_p obtained for SIGMA-ALDRICH castor oil in the case $\alpha_a = \alpha_p + 45°$ and modulating field of frequency 417 Hz. Circles: the experimental data, curve: the interpolation fit

5. CONCLUSIONS

The value of the linear birefringence $|n_{03} - n_{01}| = 2.2 \cdot 10^{-7}$ obtained in this work is similar to the value $1.6 \cdot 10^{-7}$ for medicinal castor oil by PROLAB measured previously by another static method [1]. In the case of the dichroism, the discrepancy between the result $|T_f - T_s| / \overline{T} = 0.9 \ldots 1.0 \cdot 10^{-2}$ obtained in this study and the value $3.6 \cdot 10^{-2}$ from Ref. [1] is much greater. However, such a large discrepancy does not necessarily indicate an error in one of the measurement methods and a further study is needed concerning comparison of the both methods and the effect of oxidation products in the oil on the results of measurements.

The measurement method proposed in this paper requires the value of the Kerr constant, which must be measured using other method. However, this should not be a problem in a reliable quality control system, which should include several optical constants which have a strong relationship with the purity of the oil, including also the Kerr constant.

The method described in this work may be adapted for liquids belonging to other Curie groups, which allow for the linear birefringence. However, in the case of liquids described by the ∞ Curie group the method should take into account the linear electro-optic effect, which, as we expect, will dominate the quadratic one.

REFERENCES

[1] **Izdebski M., Ledzion R., Górski P.,** Sci. Bull. Lodz Univ. Tech., s. Physics, **33** (2012) 39.
[2] **Izdebski M., Ledzion R., Górski P.,** "Measurement of quadratic electrogyration effect in castor oil", in review in Optics Communications.
[3] **Babu S., Sudershan R.V., Sharma R.K., Bhat Ramesh V.,** JAOCS, 73 (1996) 397.
[4] **Stępień M., Ledzion R., Górski P., Kucharczyk W.,** Sci. Bull. Lodz Univ. Tech., s. Physics, **33** (2012) 89.
[5] **Abu-Taha M.I., Halasa M.A., Abu-Samreh M.M.,** Journal of Modern Physics **4** (2013) 230.
[6] **Sirotin Yu.I., Shaskolskaya M.P.,** Fundamentals of crystal physics, Mir Publishers, 1982.
[7] **Izdebski M., Ledzion R., Kucharczyk W.,** Sci. Bull. Lodz Univ. Tech., s. Physics, **34** (2013)
[8] **Tomkins H.G., Irene E.A.,** Handbook of Ellipsometry, William Andrew, 2005, p. 121.
[9] **Maldonaldo T.A., Gaylord T.K.,** Appl. Opt., **28** (1989) 2075.
[10] **Ratajczyk F.,** Dwójłomność i polaryzacja optyczna, Oficyna Wydawnicza Politechniki Wrocławskiej, Wrocław 2000.
[11] **Ścierski J., Ratajczyk F.,** Optik (Stuttgart), **68** (1984) 121.
[12] **Izdebski M.,** J. Appl. Cryst., **45** (2012) 950.
[13] **Nowakowski K., Perek A., Izdebski M., Ledzion R., Górski P.,** this volume.

MODULACYJNA METODA POMIARU BARDZO SŁABEJ DWÓJŁONOŚCI LINIOWEJ I DICHROIZMU W CIECZACH NA PRZYKŁADZIE OLEJU RYCYNOWEGO POMIĘDZY METALOWYMI ELEKTRODAMI

Streszczenie

Zaproponowano metodę pomiaru bardzo słabej dwójłomności liniowej rzędu 10^{-7} i dichroizmu w cieczach opartą na technice polaryzacyjno-optycznej. Cechą charakterystyczną metody jest taki wybór konfiguracji układu, w którym możliwy jest pomiar kombinacji dwójłomności liniowej i efektu elektro-optycznego oraz kombinacji dichroizmu z efektem elektro-optycznym. Połączenie efektów niewykazujących szybkich zmian w czasie z efektem zależnym od zmiennego pola modulującego pozwoliło na poprawę czułości metody (w porównaniu do starszej metody statycznej) przez zastosowanie woltomierzy typu lock-in, które mierzą z wysoką selektywnością tylko wybraną harmoniczną. Rozważania teoretyczne zostały zilustrowane wynikami pomiarów dla oleju rycynowego.

SCIENTIFIC BULLETIN OF THE LODZ UNIVERSITY OF TECHNOLOGY
No. 1192 Physics, Vol. 35 2014

SYLWESTER KANIA[1,2]
[1]Institute of Physics, Lodz University of Technology
ul.Wólczańska 219, 93-005, Łódź, Poland
[2]Centre of Mathematics and Physics, Lodz University of Technology
al. Politechniki 11, 90-924 Łódź, Poland

HOLE DRIFT MOBILITY IN ANTHRONE AND ANTRACHINONE LAYERS WITH DIFFERENT STRUCTURE

The hole drift mobilities were measured with use of time of flight method (TOF) for layers of antrachinone and anthrone with different structural orders. The differences in the values of mobility for anthrone and anthrachinone are explained as an effect of different permanent dipole moment for these molecules.

Keywords: polycrystalline films, quasi amorphous films, amorphous films, anthrone, antrachinone, hole drift mobility, carrier transport.

1. INTRODUCTION

This paper analysis hole transport in the case of two organic materials which differ with the molecular dipole moment. There is a lack of the first-principles analytic theory explaining charge carrier mobility for condensed organic semiconducting materials over a wide range of physical material parameters, such as presence of the molecular dipole moment. Understanding the role of charge localization and energetic disorder connected with the presence or absence of the molecular dipole moment in the charge transport through these materials is crucial to enable rational design for applications of organic devices. Polycrystalline and amorphous materials posses defects at boundaries between crystalline grains. But the fundamental nature of the condensed organic materials, made of isolated, independent molecules held

together by weak van der Waals bonds, makes the presence of non-periodicity introduced by the limits of grains negligible. Such a phenomenon is possible due to the fact that molecular condensed materials are made of the atomically ordered nearly individual units-molecules, and there are no-dangling covalent bonds. The presence of the of the weak dipole and quadrupole interactions may act to localise electronic states.

This article concerns the problem of the presence of the molecular dipole moment as a source of the differences in the hole transport for the thin layers of acenes. This was the reason for whose research has been undertaken on the layers of a different arrangements of the molecules that is polycrystalline, quasi-amorphous and amorphous. The study focused on two compounds, antrachinone and anthrone, each of which has a different dipole moment, but both compounds condensed with nearly identical crystalline structure.

2. EXPERIMENTAL AND RESULTS

The measurements were made in the ambient atmosphere in room temperature using time of flight (TOF) spectroscopy [1]. The samples were made in the planar layered structure (named "sandwich" structure). There were taken *I-t* current characteristics forced with photoexcitation of electron-hole carriers near the semitransparent electrode in the presence of biasing electrical field.

2.1. Structures of antrachinone and anthrone

The parameters of nearly the same structures of antrachinone, $C_{14}H_8O_2$, and anthrone, $C_{14}H_{10}O$ [2] are presented in Table 1.

Table 1

compound	Space group	Lattice constant, [Å]	Lattice angle β [degree, min]	Dipole moment, [D]
Antrachinone ($C_{14}H_8O_2$)	$C_{2h}^5(P2_1/a)$	a_0 = 15,8, b_0 = 3,94 - 3,99 , c_0 = 7,865(10)	102º˝43´(2´)	0,6 (in benzene)
Anthrone ($C_{14}H_{10}O$)	$C_{2h}^5(P2_1/a)$	a_0 = (15.80±0.03), b_0=(3.998±0.005), c_0 = (7.86±0.16)	101º˝40´(10´)	3,66 (in benzene)

2.2. Sample preparation

Methods for preparation of the layers are described in [3, 4]. The exemplary X-diffractograms of the layers under investigation are presented in Figs. 1 and 2.

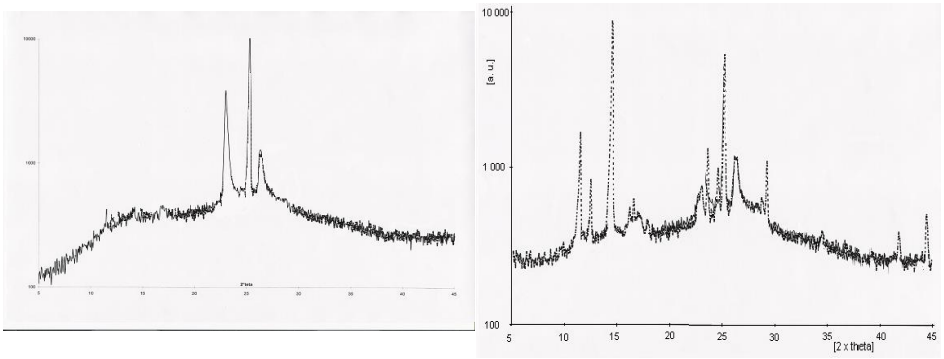

Fig. 1. Diffraction pattern (X ray) for quasi-amorphous (left) and polycrystalline (right) anthrone layers

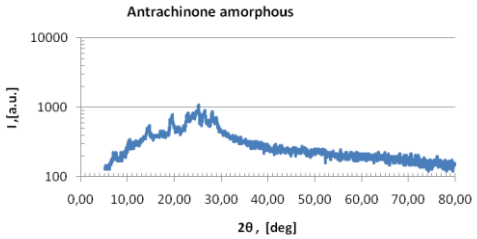

Fig. 2. Diffraction pattern (X-ray) for amorphous antrachinone layer

2.3. Measurements

Measuring procedures used for obtaining TOF transients are described in [5]. Exemplary shape of the transient *I-t* is presented in the Fig. 3. It is seen that such a shape allows the direct determination of the mobility.

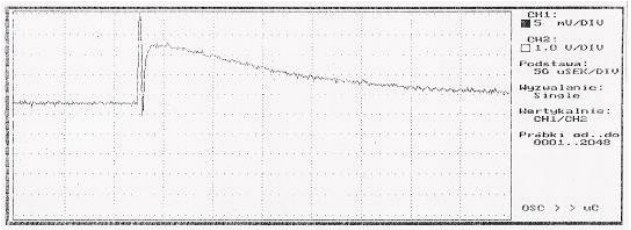

Fig. 3. Typical current pulse for amorphous antrachinone layers (U = 240 V, L = 29 μm)

2.4. Results

Obtained TOF captures of current-time pulses, allowed estimation the value for the time of flight (t_t) for measuring samples. For the more precision determination of the t_t value, obtained transients were transformed into log-log scale. All the obtained results are summarized in Table 2, where μ is drift mobility, and E_a is activation energy.

Table 2

Compound	structure	μ, [cm^2/Vs]	E_a, [eV]
antrachinone	polycrystalline	$(8 \pm 2)\cdot 10^{-4}$	0,03
	quasi-amorphous	$(3 - 7)\cdot 10^{-4}$	0,03
	amorphous	$(0{,}9 - 6{,}0)\cdot 10^{-4}$	0,03
anthrone	polycrystalline	$(7\pm2)\cdot 10^{-3}$	0,03
	quasi-amorphous	$(3 - 7)\cdot 10^{-3}$	0,03
	amorphous	$(0{,}6 - 4{,}0)\cdot 10^{-3}$	0,03

The low value of drift mobility for both molecular compounds and low activation energy suggest that the hopping charge transport takes place in the narrow band of localised states at the Fermi level.

3. CONCLUSIONS

From obtained results is seen (Table 2) that for the polycrystalline and quasi amorphous layers the values of hole mobility for anthrone (μ = 3,6 D) is of one order of magnitude higher than for antrachinone (μ = 0,6 D). For the amorphous layers high dispersion of results was obtained. However the trend line indicate a slightly higher value for anthrone layers. High dispersion of the mobility values for the amorphous layers should be caused by the partial layer's recrystallization process during measuring experiment. It was impossible to univocally evidence this recrystalization. Perhaps this results were under impact of the conditions of the execution of the experiment, that is in the ambient atmosphere and under influence of air composition. The impact of such conditions on evidence was recognized in the [1]. Based on the obtained results it could be built the hypothesis, that for the increased mobility of anthrone layers is responsible the presence of the considerable value of dipole moment, in comparison to its lack for the antrachinone layers.

The choice of the Hamiltonian in the situation described in this article is connected with the fact that nuclear dynamics is much slower than the dynamics of charge carriers and the fact that electronic coupling is weak. Hamiltonian for charge transport should be connected with static disorder, based on the

assumption on the electronic density of states and on the hopping rates between localized states.

For low density materials one-electron Hamiltonian is convenient for presentation the different kinds of charge carriers motion [7]:

$$H = H_0 + H_1 + H_2 + H_3 + H_4 \tag{1}$$

where:

$$H_0 = \sum_n \varepsilon a_n^+ a_n + \sum_\lambda \hbar\omega_\lambda \left(b_\lambda^+ b_\lambda + \frac{1}{2} \right),$$

$$H_1 = \sum_n \sum_m J_{nm} a_n^+ a_m ,$$

$$H_2 = \sum_\lambda \sum_n g_{n\lambda}^2 \hbar\omega_\lambda a_n^+ a_n \left(b_\lambda + b_{-\lambda}^+ \right),$$

$$H_3 = \sum_n \sum_{\substack{m \\ n \neq m}} \sum_\lambda f_{nm\lambda}^2 \hbar\omega_\lambda a_n^+ a_m \left(b_\lambda + b_{-\lambda}^+ \right),$$

$$H_4 = \sum_n \delta\varepsilon_n a_n^+ a_n + \sum_n \sum_{\substack{m \\ n \neq m}} \delta J_{nm} a_n^+ a_m .$$

Hamiltonian H_0 represents the full energy of the system, theirs molecules and the lattice are in the excited state, but without taking into account inter-interactions. Energy of excited state of a molecule in the defined lattice site is described with ε, its variations are described with $\delta\varepsilon_n$. The variation of ε is connected with non-phonon dispersion of energy states (diagonal elements H_{nn} of the Hamiltonian matrix). Non-diagonal elements δJ_{nm} (nm-element in the Hamiltonian matrix), represents the non-diagonal disorder of the force of interactions between two lattice nodes, but without presence of phonons (for example connected with disorder due to dipol-dipol orientation). a_n^+, a_n are followingly the operators of creation and annihilation of excited electron with energy ε in the node n., and b_n^+, b_n are followingly the operators of normal oscillations with energy $\hbar\omega_\lambda$ interact with electron in the state n and $g_{n\lambda}$ is non-dimensional coupling constant for this interaction. Transfer Hamiltonian H_1 describes electron transfer from node (n) to node (m) with overlapping energy J_{nm}. Terms H_2 and H_3 are described the impact of the lattice vibrations on the electron flow. The last H_4 is divided into two disorder terms, first one is responsible for statistical diagonal disorder and the second one for statistical non-diagonal disorder.

Dipole-dipole interactions energy between the dipol ds_1 in the centre of the coordinate system having direction s_1 in the field originated from the network

of point dipoles with directions s_n is shown below in the form of the sum of interactions with all other dipoles [6]:

$$\delta J_{1\alpha} = \frac{d^2}{2} \sum_{n=2}^{\infty} \left[\frac{s_1 s_n}{|r_{1n}|^3} - \frac{3(s_1 r_{1n})(s_n r_{1n})}{|r_{1n}|^5} \right], \tag{2}$$

where: s_1, s_n, r_{1n} are wectors, r_{1n} is a position of *n*-th dipole, α-sign a manifold of the network of point dipoles. This energy may be an element for the second term in the Hamiltonian H_4. In the case of antrachinone, with the molecules with natural dipole moment measured in benzene of 0,6 D ($2{,}00 \cdot 10^{-30}$ Cm) [1], this energy is in the order of $10^{-5} \div 10^{-6}$ eV, that is in three orders of magnitude less than the van der Waals potential energy (estimated in the range of $10^{-3} \div 7 \cdot 10^{-2}$ eV), but anthrone molecules possess a significant natural dipole moment, when measured in benzene is of 3,66 D ($1{,}22 \cdot 10^{-29}$ Cm) [1] and in this case the energy of dipol-dipol interaction can be in the order of $10^{-2} \div 10^{-3}$ eV, does it mean the value comparable to the van der Waals potential. These additional dipol-dipol energy present for anthrone structures can lead to broadening of the bands in the condensed form and to the enhanced overlapping of the wave functions for the charge carriers conducting via localized states.

In the high temperature limit, the transfer rate for a charge to hop from a site i to a manifold of final sites α is [8]:

$$k_{i\alpha} = \frac{2\pi}{\hbar} \frac{J_{i\alpha}^2}{\sqrt{4\pi\lambda_{i\alpha} k_B T}} \exp\left[-\frac{(\Delta E_{ij} - \lambda_{i\alpha})^2}{4\lambda_{i\alpha} k_B T} \right], \tag{3}$$

where T is temperature, $\lambda_{i\alpha} = \lambda_{i\alpha}^{\text{int}} + \lambda_{i\alpha}^{out}$ is the reorganization energy, which is a sum of intra- and intermolecular (outersphere) contributions, $\Delta E_{i\alpha}$ is the lattice nodes-energy difference.

For both molecular compounds in condensed state obtained values of the mobility are below 10^{-2} cm^2/Vs, and the estimated values of the activation energy are the same.

Despite of almost the same crystallization structure (the space group $C_{2h}^5(P2_1/a)$ operates for both), clear differences in the magnitude of mobility were observed. For anthrone, with molecule possessing a natural dipole moment, the mobility of holes in the condensed state is almost one order of magnitude greater than that measured for antrachinone this fact can be connected with the higher value of transfer rates taking into account in the term H_4 of Hamiltonian. The more precise determination needs further studies on the influence of the structural disorder on the mobility value.

Acknowledgements

Great thanks to prof. B. Marciniak and prof. M. Wieczorek for preparation of the spectral grade antrachinone and anthrone and for enabling the Roentgen analysis and to prof. J. Świątek for valuable discussions.

REFERENCES

[1] **Kania S., Kondrasiuk J., Bąk G.W.**, Eur. Phys. J. E, **15** (2004) 439.
[2] **Landolt-Börnstein**, Zahlenwerte und Funktionen aus Naturwissenschaften und Technik, Springer Verlag, Berlin, 1971.
[3] **Kania S.**, Sci. Bull. Tech. Univ. Łódź, s. Physics, **28** (2007) 27.
[4] **Kania S.**, Sci. Bull. Tech. Univ. Łódź, s. Physics, **30** (2009) 65.
[5] **Kania S.**, Sci. Bull. Tech. Univ. Łódź, s. Physics, **34** (2013) 19.
[6] **Kitaigorodskii A.I.**, Molecular Crystals and Molecules, Acad. Press, N.Y. 1973.
[7] **Pope. M., Swenberg C.E.**, Electronic processes in organic crystals., Clarendon Press New Yor 1982.
[8] **Rühle V., Lukyanov A., Falk M., Schrader M., Vehoff T., Kirkpatrick J., Baumeier B.** and **Andrienko D**., J. Chem. Theory Comput., 7 (2011) 3335.

DRYFTOWA RUCHLIWOŚĆ DZIUR W WARSTWACH ANTRONU I ANTRACHINONU O RÓŻNEJ STRUKTURZE

Streszczenie

Poddano analizie wartość ruchliwości dziur w polikrystalicznych, quasi-amorficznych i amorficznych warstwach antronu i antrachinonu. Materiały wyjściowe były o czystości spektralnej. Oba związki krystalizują w identycznej strukturze $C_{2h}^5(P2_1/a)$ krystalograficznej układu skośnego o prawie identycznych stałych sieciowych i prawie identycznym kącie β. Dla warstw antronu, którego cząsteczki posiadają stały moment dipolowy, uzyskano prawie o rząd większą wartość ruchliwości niż dla warstw antrachinonu, niezależnie od stopnia uporządkowania tych warstw. Próbujemy sformułować hipotezę i wykazać jej słuszność, że za prawie o rząd większą ruchliwość dziur w warstwach antronu odpowiada obecność znacznego momentu dipolowego w cząstkach tego związku.

SCIENTIFIC BULLETIN OF THE LODZ UNIVERSITY OF TECHNOLOGY
No. 1192 Physics, Vol. 35 2014

SYLWESTER KANIA[1,2] , JANUSZ KULIŃSKI[2]
[1]Institute of Physics, Lodz University of Technology
ul. Wólczańska 219, 93-005, Łódź, Poland
[2]Centre of Mathematics and Physics, Lodz University of Technology
al. Politechniki 11, 90-924 Łódź, Poland

CORRELATED NETWORKS IN THE ADSORPTIONENHANCED CURRENTS

Injection of carriers into thin layers of acenes due to adsorption of ethanol activator molecules is considered as a electron transfer reaction between two phases. Complexity of the processes may be diminished with applying electron transfer theory in the meaning of Marcus.

Keywords: tetracene films, p-quaterphenyl films, adsorption, electron transfer reactions.

1. INTRODUCTION

Organic thin layers made of the acenes have broad applications in many fields of modern microelectronics. Especially, the deep modulation of the conductivity due to the adsorption-induced electron transfer processes at the interface between organic solid state layer and gaseous activator is under great interest of gas sensor technology. An efficient application for organic materials requires very good understanding of the dynamic interactions of the solid surface with the molecules of ambient vapour. It may be noticed that conductivity enhanced adsorption process becomes similar to the catalysis. In our experiments the reactants exchange the charge with the solid phase and then they are transformed into the substrates (molecules or ions), but the molecules belonged to the solid phase are subjected to the reversible transformations in the run of the carriers forced by the electromotive force (EFM) existing in the measuring circuit. For the reason of electronic phenomena all the described process can be compared to the principle of operation for the bipolar transistor where the active absorbing surface acts as a basis injected carriers.

Consequently, interesting reactions are that which conduct to the short range interactions with excitons or other forms for transferring the charge existing on the surface of the solid phase connected with possibility of transferring this charge into the volume of the layer. Such a description of the process of enhancing current due to adsorption was presented in [1], and then developed [2] in connection with new conceptual theory of abrupt transition in the structural formation of interconnected networks [3, 4]. There is a some number of reports devoted to independent transfer of the small molecules to the absorbing solid organic surface with the energetic disorder and structural roughness (for example [5]) with use of Monte Carlo simulations, but these papers do not touch problem of injection of charges during adsorption.

Absorption of the ethanol and other alcohols on the hydrocarbon films carbonized at high temperature was examined with use of infra-red spectroscopy [6]. Such a methodology allows to establish which atoms or group of atoms of adsorbate and absorbent react mutually in the process of adsorption. In the result of this explorations it was found that the adsorbed molecules had been formed the wide band of the stretching oscillations O-H (3550 cm^{-1}), which widening is connected with creation of H bonds. Apolar group of adsorbed ethanol forms the stretching bands C-H in the region of 2990 and 2820 cm^{-1}. Forming the band at 1480 cm^{-1} (not existing for the gas molecule) points out that a fraction of ethanol is absorbed with cooperation of apolar group C_2H_5 to the weakly oxidized surface. Above data indicate the multichannel adsorption process, so in that reason point to the coexistence of several competitive processes, and only part of them leads to the interactions with the layer molecules connected with transfer of the carriers. Complexity of the whole problem allows however use the simplifying concept of Marcus'es electron transfer reactions theory [7,8]. This observation coincides with our proposed model in that and earlier papers [9-12].

2. EXPERIMENTAL

Thin films of polycrystalline tetracene ($C_{18}H_{12}$) and of p-quaterphenyl ($C_{24}H_{18}$) made as a measuring cells of "sandwich" type with Au – Al electrodes were prepared with vacuum deposition method under the pressure of the order of 10^{-5} Torr on glass plates covered with metal film. During evaporation the evaporation rates were kept in the range 20÷30 Å/s. The substrate temperatures were about 300 K and obtained layers were in the thickness range from 15 μm to 17 μm. Structural examinations of the obtained layers were made using X-ray diffraction with an automatic diffractometer DAR in the 2θ range from 5º to 80º with measuring step 0.05º. Direct measurements of the current response for the

interface adsorption process were fulfilled in the set up shown in the Figure 1. The measuring cell was fixed in the vacuum flask with controllable ethanol vapour flux getting out from the source with the vapour pressure of 10^{-2} Tr. The first and the another doses of the vapour were controlled with precision gas-inlet valve. New dose of vapour makes the current to continue the increase and the saturation was realized in the higher level. The characteristic kinetics of the current for tetracene film vaporized with C_2H_5OH is presented in Fig. 2.

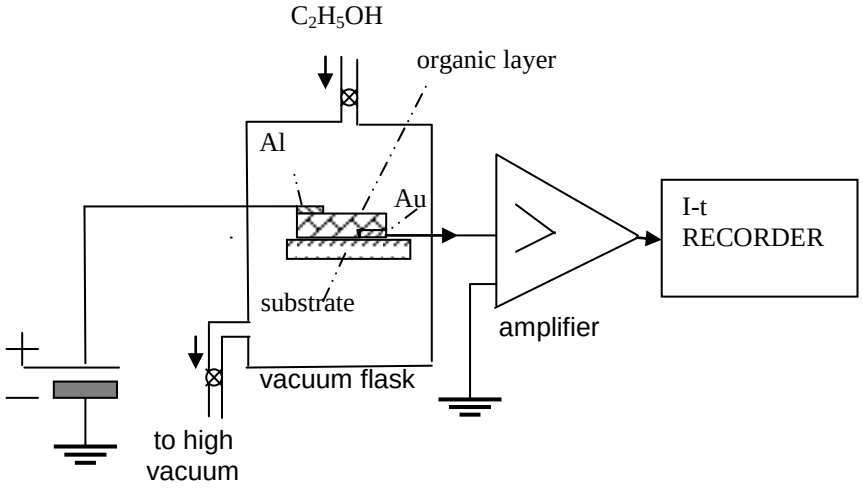

Fig. 1 Experimental setup

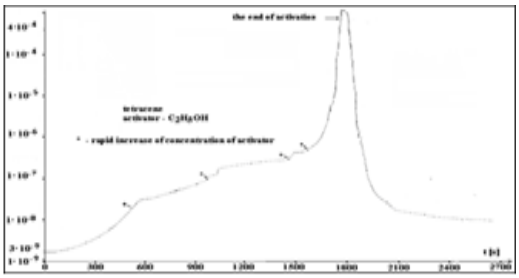

Fig. 2. Effect of added ethanol on absorption-current in the anthacene layer (thickness 15 μm, active surface area 0,5 cm^2)

3. DISCUSSION

Discussion is divided into two kinetics problems, first is the nature of kinetics of the adsorption, and second is how the adsorption process influence the kinetics of the electron transfer in the interface. The adsorption process is studied in the vacuum where the competition of different kinds of molecules is eliminated. But even in such defined case the competition of decomposition products originated from the ethanol vapour exists. Ethanol at 300 K slightly decomposes, and the main decomposition products appeared in the equilibrium conditions [13] are acetaldehyde – CH_3CHO (2%) and H_2O (6%) and intact ethanol (92%). At 300 K other decomposition products as C_2H_4, CO_2, C_2H_6 may be produced. The mixture entered to the reactor flask will be under influence of the disrupting potential [14] existing between dangling vicinal rings of the layer molecules. Such an interaction in the range of 0.5 eV is able to make additional decomposition of the vapour molecules. In the low temperature conditions ethanol gas undergoes dehydration step so acetaldehyde may be present in the reactor. The absorbed hydrogen atoms are able to mediate to transfer electrons to the dangling rings of the molecules placed in the irregularities of the layer [5]. The probable sequence of reactions can be expressed as follows:

$$CH_3CH_2OH \rightarrow CH_3CHO + 2H_{ads} + 2e^{-}.$$

The O-H bound of hydroxyl group of ethanol is already activated resulting with the oxygen atom bonding to the surface:

$$OH + OH \rightarrow H_2O + O_{ads}\ .$$

Oxygen atom absorbed at surface can absorb an electron from layer molecule creating a new transport charge – hole. This process is possible because in the equilibrium the mixture may contain H_2O. Adsorbed oxygen can enhance the chemisorptions of ethanol [6]. Such a mechanism is consistent with the earlier works [15] where it was revealed growth of conductivity in the layers of tetracene and p quaterphenyl in the presence of external atmosphere of O_2, H_2O.

Treating the whole process as a reaction of the electron transfer, the adsorption enhanced current may be considered as the charge flow between molecules of ethanol in vapour phase to the molecules of condensed layer. And in the set-up presented in Fig. 1 the measured characteristics can be considered as resulting from injection of electrons into the film.

The saturation levels of the currents after every vaporization are important because they are directly correlated with the rate of electron transfer at the interface and may be considered as proportional to the number of electrons which cross the interface existing at the surface of the layer. The rate of electron-transfer can be calculated easily by integration the *I-t* curve. Similar shape of dependence for absorption of ethanol was observed in [6] in the function

of relative pressure (relative to the pressure of saturated vapour-$p_0 \approx 44$ Tr). The process was rapid and linear with the growth of a pressure for low relative pressures (in the order of $0{,}1p/p_0$) what can be explained as a confirmation for the high energy of adsorption interactions with organic solids for this alcohol. Making an assumption that an excited acene molecules at the surface are produced by direct electron injection at the solid surface array or by exciton migration from interior of the crystal to the surface we can consider the whole process as a reaction with reaction cross section σ_e for the p-quaterphenyl (anthracene) – ethanol system. In that limits the following estimation can be valid roughly:

$$\sigma_e = \sigma_g \cdot Q_{ex} \cdot \frac{1}{\tau \cdot N_v}, \tag{1}$$

where σ_g is geometrical cross section of a site of surface lattice with acene molecule of the film, Q_{ex} is the reaction yield per exciton reached at the surface, τ is approximated by exciton lifetime in the bulk layer, N_v – number of collisions of adsorbate in the interface layer. Substituting the numerical values $\sigma_g = 50$ Å^2, $Q_{ex} = 1$, $N_v = 1{,}5 \cdot 10^{14}$ cm^{-2}s^{-1}, $\tau = 4 \cdot 10^{-9}$ s, σ_e is roughly equal to $2 \cdot 10^{-6} \cdot \sigma_g$. It conduct to the conclusion that the reaction was limited the number of collisions in the interface.

For observed systems the time dependence of desorption current and obtained value of entropy for sorption, for tetracene ΔH=84 kJ/mol and for p-quaterphenyl ΔH = 77 kJ/mol, may points out that two mechanisms are present: physic sorption and weak chemisorption.

In the previous paper [2] we have discussed the phenomenon of adsorption in the scope of the model of abrupt transitions in the structural formation of two undirected interconnected networks with the same number of nodes [3,4] and developed in [16] and in the scope of this model is needed a description using the Hamiltonian in the manner of sum of terms centered on the active lattice nodes of the layer.

4. CONCLUSIONS

If we consider 2-D localized gas layer at the interface interacted with molecules of condensed layer then we can in terms of semi-classical Marcus's theory charge transfer rate may be interpreted as reaction rate for change ionization states between adjacent molecules. The decisive parameter for charge transport between molecules in the interlayer is intermolecular transfer integral J_{ij}, that express the possibility of transfer of charges between interacting

molecules. For adjacent molecules the transfer integral may be evaluated from Schrödinger equation. Making use of Fermi golden rule for describing the resonant transition from initial state |i> located in the 2-D gas layer in the interface to a final manifold of discrete states |α> with energies E_α located in the solid layer under the influence of a time- independent perturbation, the transfer rate between initial state *i* and a final states *α* is given by [7]:

$$k_{i\alpha} = \sum_{\alpha} k_{i\alpha} = \frac{2\pi}{\hbar} \sum \left| J_{i\alpha} \right|^2 \delta(E_i - E_\alpha) \tag{2}$$

where: $J_{i\alpha} = \langle i|U|\alpha \rangle$ is a perturbation matrix element between the initial state and one of the final states, and δ function ensures energy conservation during the transition between the initial and final states.

In the high temperature limit, the transfer rate for a charge to hop from a site i to a manifold of final sites α is [8]:

$$k_{i\alpha} = \frac{2\pi}{\hbar} \frac{J_{i\alpha}^2}{\sqrt{4\pi\lambda_{i\alpha} k_B T}} \exp\left[-\frac{\left(\Delta E_{ij} - \lambda_{i\alpha}\right)^2}{4\lambda_{i\alpha} k_B T} \right], \tag{4}$$

where T is temperature, $\lambda_{i\alpha} = \lambda_{i\alpha}^{\text{int}} + \lambda_{i\alpha}^{out}$ is the reorganization energy, which is a sum of intra- and intermolecular (outersphere) contributions, $\Delta E_{i\alpha}$ is the site-energy difference, and $U_{i\alpha}$ is the electronic coupling element.

ACKNOWLEDGEMENTS

Great thanks to prof. B. Marciniak and prof. M. Wieczorek for preparation of the spectral grade antrachinone and anthrone and for enabling the Roentgen analysis, and to prof. J. Świątek for valuable discussions.

REFERENCES

[1] **Kania S., Kuliński J.**, Sci. Bull. Technical University of Lodz, Physics, **30**, (2009) 47.
[2] **Kania S., Kuliński J.**, Sci. Bull. Technical University of Lodz, Physics, **34**, (2013) 35.
[3] **Brandão F.G.S.L.** and **Horodecki M.**, Nature Phys., **9** (2013) 721.
[4] **Radicchi F., Arenas A.**, Nature Phys., **9** (2013) 717.
[5] **Kuchta B., Firlej L., Marzec M.** and **Boulet P**., Langmuir, 24 (2008) 4013.

[6] **Zawadzki S.**, Spektroskopia w podczerwieni zjawisk powierzchniowych na węglach (Infrared spectroscopy of the surface phenomena on carbons) (UMK, Toruń 1980).
[7] **Martinelli N.,** Charge transport in organic conjugated materials:impact of lattice dynamics and coulombic interaction effects, Univ de Mons dissertation, 2011.
[8] **Rühle V., Lukyanov A., Falk M., Schrader M., Vehoff T., Kirkpatrick J., Baumeier B.** and **Andrienko D**., J. Chem. Theory Comput., 7 (2011) 3335.
[9] **Kania S., Kuliński J.,** Sci. Bull. Technical University of Lodz, Physics **32**, (2011) 23.
[10] **Kania S., Kuliński J.**, Chem. Met. Alloys, **4** (2011) 31.
[11] **Kania S., Kuliński J.**, Sci. Bull. Lodz University of Technology, Physics, **33** (2012) 65.
[12] **Kania S., Kuliński J.**, Sci. Bull. Technical University of Lodz, Physics, **31** (2010) 51.
[13] **Cheong H.W., Lee M.J.**, J. Ceram. Proc. Res. Vol. 7, No. 3 (2006) pp. 183.
[14] **Levitt M., Perutz M.F.**, J. Mol. Biol., **201** (1988) 751.
[15] **Kania S., Kondrasiuk J., Bąk G.W**., Eur. Phys. J. E, **15** (2004) 439.
[16] **Reis S.D.S., Hu Y., Babino A., Andrare Jr J.S., Canals S., Sigman M.,** and **Makse H.A.,** Nature Phys., **9** (2013) 721.

SKORELOWANE SIECI W PRĄDACH WZMOCNIONYCH ADSORPCJĄ

Streszczenie

Badano proces aktywacji i proces transportu elektronów w warstwach tetracenu i p-kwaterfenylu. Złożoność procesów towarzyszących przepływowi prądu wzmacnianego adsorpcją wymaga modeli upraszczających. Możliwość zastosowania modelu gwałtownych przemian w tworzeniu strukturalnym oddziałujących wzajemnie sieci prowadzi do możliwości zastosowania hamiltonianu będącego sumą hamiltonianów dla każdego z kanałów transferu ładunku. Stwarza to możliwość zastosowania koncepcji szybkości transferu ładunków na bazie teorii Marcusa reakcji z transferem elektronów.

SCIENTIFIC BULLETIN OF THE LODZ UNIVERSITY OF TECHNOLOGY
No. 1192 Physics, Vol. 35 2014

**SYLWESTER KANIA[1,2], JANUSZ KULIŃSKI[2,3] ,
BERNARD MARCINIAK[3] , EWA RÓŻYCKA-SOKOŁOWSKA[3]**
[1]Institute of Physics, Lodz University of Technology
ul.Wólczańska 219, 93-005, Łódź, Poland
[2]Centre of Mathematics and Physics, Lodz University of Technology
al. Politechniki 11, 90-924 Łódź, Poland
[3]Institute of Chemistry, Environmental Protection and Biotechnology
Jan Długosz University in Częstochowa
al. Armii Krajowej 13/15, 42-200 Częstochowa, Poland

BIPOLAR TRANSPORT OF CHARGE CARRIERS IN THIN FILMS OF 9,10-DIMETHYLANTHRACENE AND 1-ACENAPHTHENOL

The current-voltage (I-U) characteristics we have been measured for thin films of 1-acenaphthenol and 9,10-dimethyl-anthracene prepared from their commercially available materials as products with purity ≥ 10^{-3} mass %. Using the method of differential processing of the characteristics, charge transport mechanism in these films was assessed.

Keywords: 1-acenaphthenol, 9,10-dimethylanthracene, conductivity, electric characterization.

1. INTRODUCTION

Recently one can observe constantly increasing interest to thermally stable low molecular derivatives of polycyclic aromatic hydrocarbons (PAHs) to which the title 1-acenaphthenol (1-Acol) and 9,10-dimethylanthracene (9,10-DMA) (their known crystal structures were redetermined by one of us [1, 2]), also belong. The interest is mainly connected with a very interesting optical and opto-electrical properties of this group of compounds, and especially the charge and energy transport properties owing to which they are now treated as one of the most promising active materials for a new generation of low-cost, flexible

electronic and opto-electronic devices. The most intensively studied prototypes of these devices, in which a number of different PAH derivatives in the form of technologically preferred thin films are tested as active materials, are organic light emitting diodes (OLEDs), organic field-effect transistors (OFETs) and photovoltaic and solar cells [3-8]. In the case of such weakly bonded organic active materials, the charge and energy transport properties are, however, very sensitive not only to physical imperfection of their films but, first of all, to chemical impurities contained in them, even if their concentration is on ppm or sub-ppm scale [9-11]. Therefore, high purity is of extreme importance for obtaining meaningful results for all questions, which are connected with energy and charge transfer.

In our previous paper [12], the preliminary results of electric characterization of both aforementioned materials were interpreted on the basis of the classic theory of space charge limited currents (SCLC) [13]. As a result, it has been found that in the case of 1-Acol, the concentration of the traps lies in the range of $2 \cdot 10^{11} \div 1 \cdot 10^{14}$ cm^{-3}, while for 9,10-DMA this concentration reaches a value of $9 \cdot 10^{14}$ cm^{-3}. It has also been observed that the measured *I-U* characteristics became fully stable only when the field strength reached the values from the range of $2 \cdot 10^{6}$ V/m to $2 \cdot 10^{7}$ V/m. Simultaneously resistivity of the layers were on the levels of $1.0 \cdot 10^{11} \div 9.0 \cdot 10^{12}$ and $6 \cdot 10^{11} \div 1.4 \cdot 10^{12}$ Ωm for 1-Acol and 9,10-DMA, respectively.

In this paper, based on the experimental results obtained in the frame of work cited above, and using the method proposed by Manfredotti at al. [14, 15], charge transport mechanism in these films was assessed.

2. EXPERIMENTAL

2.1. Materials

The starting materials were commercially available 1-Acol (purity -99%) and 9,10-DMA (pure), purchased from Aldrich and Fluka respectively. The materials were recrystalized from distilled benzene and from anhydrous ethyl alcohol, then, they were chromatographed on columns filled with Al_2O_3, and dried under vacuum. The gas chromatographic (a Hewlett Packard 5890 series II gas chromatograph equipped with a mass spectrometry detector) analysis of such purified materials has shown that the total impurity content in them is $\leq 10^{-3}$ mass %.

2.2. Measurements

The thin films of 1-Acol and 9,10-DMA were deposited in the vacuum of order of 10^{-5} Tr on an Au layer (bottom electrode) deposited earlier on the quartz glass substrate. In the same manner was also prepared the top aluminum electrode using an appropriate mask. In this way the measuring cell (see Fig. 1a) in the form of planar capacitor with the plates area of about 0.5 cm^2 was made. For such constructed capacitor the capacitance was measured (Semi-Automatic RLC Bridge type E314), in order to evaluate the thicknesses (L) of the investigated films. These thicknesses were 18.5 and 16 μm for 9,10-DMA and 1-Acol, respectively. During measurements the measuring cell was placed in the Faraday Cage (see Fig. 1b) for eliminating the electromagnetic noise. Current-voltage characteristics were obtained for the field strengths from $2 \cdot 10^5$ V/m to $2 \cdot 10^7$ V/m; an appropriate range of the biasing voltages was 3-280 V. The above characteristics were determined in the ambient atmosphere at the temperature of 300 K.

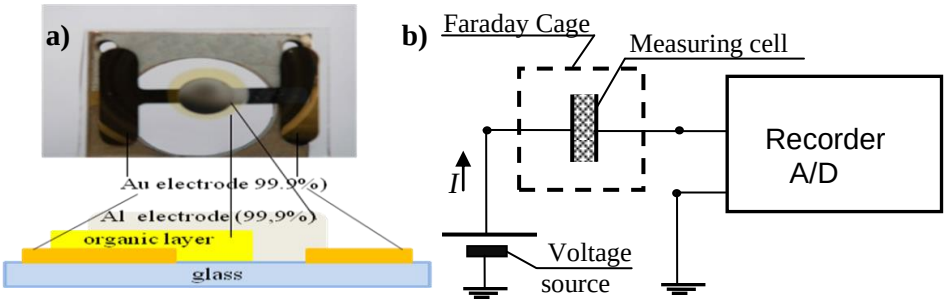

Fig. 1. The schemes of the measuring cell and its picture (a) and the measuring setup used for determination of I-U characteristics (b)

3. RESULTS AND DISCUSSION

As mentioned in the Introduction, the charge transport mechanism (holes and electrons) may be determined from a slope (α) of current-voltage characteristics (i.e. current density (J) *versus* biasing voltage (U)) defined as [14, 15]:

$$\alpha = \frac{d[\ln(J)]}{d[\ln(U)]}. \tag{1}$$

Basing on the α values, the measured *I-U* characteristics may be transformed to the α – *U* ones, which allow obtaining the mean value of charge carrier mobilities.

Figs. 2a) and b) shows *J-U* characteristics in log-log coordinates that were determined on the basis of the *I-U* characteristics measured for thin films of both investigated compounds. Instead the transformed characteristics α – *U* where the values of power exponent α were calculated from the above *J-U* characteristics according to eq. 1, are presented in Figs. 2c) and d). In the calculations, a Logger Pro Vernier Software & Technology program was used.

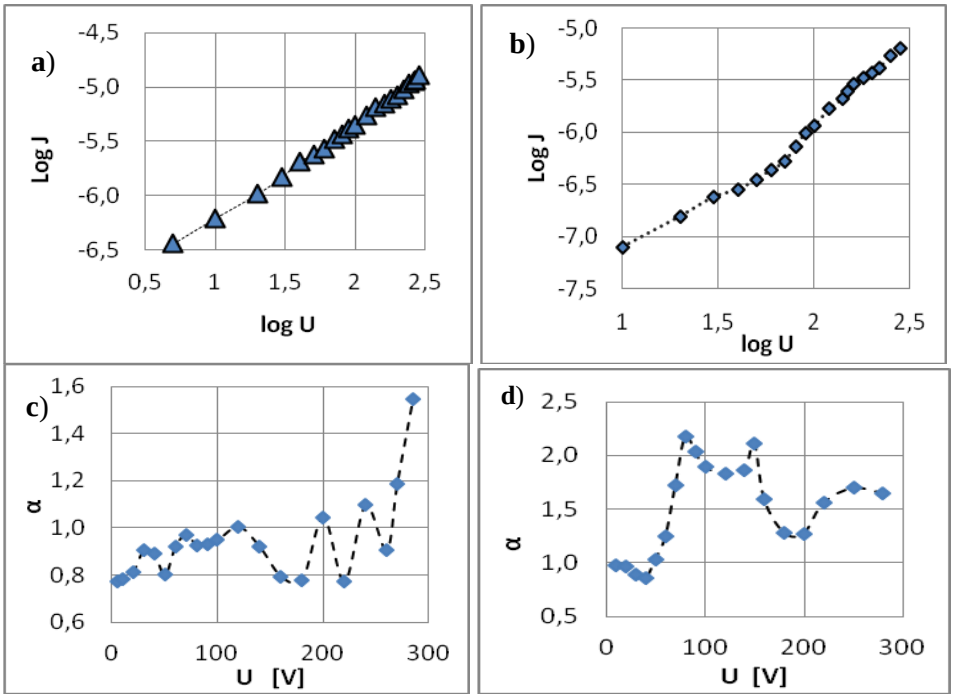

Fig. 2. Characteristics of *J versus U* calculated for 9,10 DMA (*L* = 18.5 μm) **a**) and 1-Acol (*L* = 16 μm) **b**), and their respective characteristics of α *versus U* **c**) and **d**)

Figs. 2c) and d) show that on the plots of transformed characteristics a few clear maxima (α_{max}) occur. According to the suggestion of Bagratishvilli et. al. [16], Tagyev et. al. [17] and Mikhelashivi et. al. [18] the values of α_{max} may be used for evaluation of the discrimination coefficients Q_{max} and Q_{am} defined by eq. 2 and eq. 3, respectively.

$$Q_{\max} = \frac{(2\alpha_{\max} - 1)^2 (\alpha_{\max} - 1)}{(\alpha_{\max} + 1)^2} \tag{2}$$

$$Q_{am} = \frac{(2\alpha_{\max} - 1)(\alpha_{\max} - 1)}{(\alpha_{\max})^3} \frac{\varepsilon\mu}{L^3} \frac{U_m}{J_m} \tag{3}$$

Here, U_m, J_m, ε and μ are: the voltage, the current density, the dielectric constant and the mobility in the limits of SCLC current, respectively; all these quantities correspond to α_{max}. For the calculations the values of ε were assumed to be equal 3.1 for both materials, because of similar values of polarization energy for two and three ring acenes being in the range of 1.6 eV [19], and μ was estimated from the Child's law for the SCLC currents [18].

The values of Q_{max} and Q_{am} calculated for both materials are presented in Table 1 together with the value of $4\alpha_{max}$ which is valid as a discrimination criterion for the condition for for appears field ionization (proposed in the papers [16, 18], i.e. $Q_{max}<4\alpha_{max}$).

Table 1

No.	compound	Q_{max}	Q_{am}	$4\alpha_{max}$
1	1-acenaphthenol	1.32	0.51	4.383
2	9,10-dimethylanthracene	0.031	0.23·	8.716

In the Table 2 mobilities and recombination mobilities determined from transformed current -voltage characteristics are compared with the time of flight (TOF) mean drift mobility obtained earlier by us (non-published data) for the same layers. The condition for appears field ionization i.e. $Q_{max}<4\alpha_{max}$, is fulfilled for both materials. (see Table 2).

Table 2

No.	compound	carrier mobility [cm^2/Vs]	recombination mobility [cm^2/Vs]	TOF mean drift mobility [cm^2/Vs]
1	1-acenaphthenol	4.8	1.9	1.1
2	9,10-dimethylanthracene	0.91	0.25·	0.14

For 1-Acol we obtained the condition $Q_{max}>1$, what can denotes monopolar injection. This result is in accordance with our earlier TOF measurements, where the life time for electrons was immeasurable. However, obtained Q_{am} value being on the order of one may stand for one of the three possibilities: the injection of free carriers (with recombination limited current) or field ionization of trap levels or trap free SCLC currents. For 9,10- DMA the both values of Q_{max}

and Q_{am} are clearly less than one. Therefore, this fact may be treated as an unambiguous case of double injection of free carriers.

4. CONCLUSIONS

- Basing on the results of our investigations it may be concluded that the use of obtained high purity materials has excluded the impact of impurities on the electrical characteristics. The impact of high purity is seen in high conductivities for both materials: 1-Acol and 9,10-DMA.
- For 1-Acol it was obtained more possible the unipolar mechanism of current flow but for 9,10-DMA the bipolar conductivity was unambiguously confirmed.
- The method of differential processing of current voltage used for recognition of charge flow mechanism approved its effectiveness, it was justified by comparison of the conductivity measurements with TOF method.
- It is noteworthy that phenomenon of bipolar transport is of great significance for possibility for its use in ambipolar OFETs, which are the basic element in the organic circuits such as inverters, oscillators and even recently in organic light emitting transistors.
- High bipolar conductivity for 9,10-DMA and high values of the mobilities for electrons and for holes allows us to conclude that it has a great potential for applications in organic electronics.

REFERENCES

[1] **Marciniak B**., Acta Cryst., **E63** (2007) 3183.
[2] **Marciniak B**., Acta Cryst., **E63** (2007) 1311.
[3] **Kilon J., Kim M.K., Hong J.P., Lee W., Noh S., Lee C., Lee S., Hong J.-J**., Org. Electron., **11** (2010) 1288.
[4] **Huang J., Hu B., Lam M.K., Cheah K., W., Chen C.H., Su J.-H**., Dyes and Pigments., **89** (2011) 155.
[5] **Boeg K.J., Khim D., Kim J.-H., Kang M., You I.-K., Kim D.-Y**., Org. Electron., **12** (2011) 634.
[6] **Tyagi P., Venkatesvararao A., Thomas K.R.J.,** J. Org. Chem., 76 (2011) 4371.
[7] **Kwon J., Hong J.-P., Lee W., Noh S., Lee C., Lee S., Hong J.-I**., Org. Electron., **11** (2010) 1103.
[8] **Chen R.-F., Xie G.H., Zhao Y., Zhang S.-L., Yin J., Lin S.-Y**., Org. Electron., **12** (2011) 1619.
[9] **Hoesterey D.C., Letson G.M**., J. Phys. Chem. Solids., **24** (1963) 1609.
[10] **Schmillen A., Falter W.-W**., Z. Phisik, **218** (1969) 401.
[11] **Benz K.W., Wolf H.C.**, Z. Naturforsch. **19a** (1964) 177.

[12] **Kania S., Kuliński J., Marciniak B., Różycka-Sokołowska E.**, Sci. Bull. Tech. Univ. Lodz, No. 1183 Physics **34** (2013) 35.
[13] **Čapek V., Muzikante I.**, Electronic states in organic molecular crystals., in Organic Electronic Materials **eds.: Farchioni R., Grosso G.**, Springer-Verlag Berlin Heidelberg 2001, 283-322.
[14] **Manfredotti C., de Blasi C., Gallasini S., Micocci G., Buggiero L., Tepore A.**, Phys Stat, Sol, (a). **36** (1976) 569.
[15] **Mancini A.M., Manfredotti C., de Blasi C., Micocci G., Tepore A.**, Rev. Phys. Appl. **12** (1977) 255.
[16] **Bagratishvilli G.D., Dzanelidze R.B., Jishiashvilli D.A., Piskanovskii L.V., Zyuganov A.N., Mikhaelashvilli V.N.** and **Smertenko P.S.**, Phys. Stat. Sol. (a) **65** (1981) 701.
[17] **Tagyev B.G., Asadullayeva C.G.**, Phys. Gov. Az. Trans. **XXX** (**2**), (2010) 154.
[18] **Mikhelashivi V., Eisenstein G.**, J. Appl Phys. **89** (**6**) (2001) 3256.
[19] **Gutman F., Lyons L.E**., Organic semiconductors. John Wiley and Sons, Inc., New York, London, Sydney 1967.

TRANSPORT BIPOLARNY W CIENKICH WARSTWACH 9,10-DIMETYLOANTRACENU I 1-ACENAFTOLU

Streszczenie

Stosując kryteria dyskryminujące zasięg występowania mechanizmów przewodzenia można postawić hipotezę, że prądy płynące przez warstwy 9,10 dimetyloantracenu są bipolarne, zaś w przypadku 1-acenaftolu prądy mogą być monopolarne lub bipolarne. Wysokie wartości ruchliwości dla obu materiałów wskazują na ich duży potencjał do potrzeb elektroniki organicznej. Bipolarność prądów płynących przez 9,10 dimetyloantracen w połączeniu ze stabilnością chemiczną i mechaniczną uzyskiwanych z niego warstw pozwala traktować ten materiał jako wysoce przydatny dla potrzeb optoelektroniki.

SCIENTIFIC BULLETIN OF THE LODZ UNIVERSITY OF TECHNOLOGY
No. 1192 Physics, Vol. 35 2014

MAGDALENA MARCINIAK, KLAUDIA HILLEBRANDT, ANNA KOMENDA, RAFAŁ LEDZION, PIOTR GÓRSKI

Institute of Physics, Lodz University of Technology
ul. Wólczańska 219, 90-924 Łódź, Poland
e-mail: rafal.ledzion@p.lodz.pl

THE EFFECT OF THE MOLECULAR WEIGHT ON THE ELECTROOPTIC KERR PHENOMENON OF METYL SILICON OIL

The Kerr constant and quadratic electrooptic coefficient in methyl silicon oils were measured. The dependence of their magnitude on molecular mass was determined. On the base of obtained results one cannot define the character of the dependence between determined quantities and molecular mass of examined oils.

Keywords: Kerr effect, quadratic electro-optic effect, organosilicon polymers, methyl silicon oils.

1. INTRODUCTION

The aim of our research is to investigate the Kerr constant and quadratic electro-optic effect in selected methyl silicone oils. Methyl silicon oils are used in many optical experiments, for example during the measurements of electro-optic effects in crystals. Hygroscopic materials may significantly change their properties since they are absorbing water from the air during the experiment. To prevent this, methyl silicon oil is used to create the protective layer around the examined crystal. What is more, the layer of oil prevents the examined crystal from mechanical destructions which may be caused by applied electric field. Such approach is essential during studies of the electro-optic effects in hygroscopic crystals.

2. METHYL SILICON OILS

Silicones are synthetic organosilicon polymers with structure of siloxanes where atoms of silicone are substituted by alkyl or aryl groups. They are obtained in the form of oils, elastomers or silicone resins [1]. The basic component constituting the polymer chain consists of silicon oxygen couple. Then, two methyl groups are attached to each silicon molecule [2]. The structural formula of methyl silicon oil molecule is shown in Fig. 1.

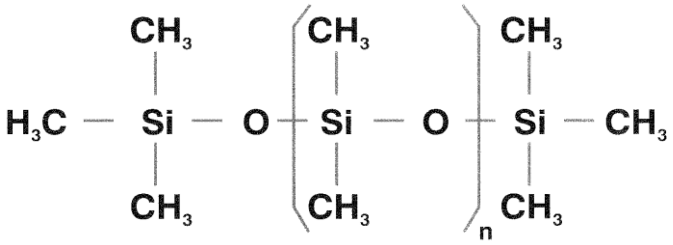

Fig. 1. The structural formula of oil molecule (*n* denotes the number of dimethyl silicone segments) [2]

In this study, methyl silicon oils produced by Organika Sarzyna SA were used. In further considerations we will use abbreviation OM and magnitude of viscosity in centistokes to denote methyl silicon oil of given viscosity. For example, the methyl silicone oil of viscosity 100 cSt will be denoted by OM 100.

3. THE DEPENDENCE BETWEEN VISCOSITY AND MOLECULAR MASS

The viscosity of methyl silicon oils depends on its molecular mass. The detailed data concerning molecular mass and viscosity are given by the producer [2]. They are shown in Table 1. The values for OM 300 and OM 3000 were determined in Ref. [3].

Table 1

Viscosity and molecular mass of methyl silicon oils [2,3]

η [cSt]	10	50	100	300	500	1000	3000	5000	10000
M [Da]	1200	3800	6000	17000	17000	28000	40000	49000	62000

4. MEASUREMENT OF KERR CONSTANT

The Kerr effect consists in appearing of birefringence in medium under influence of electric field. The effect can be observed in various media with various symmetry. For substances in which the effect is observed, the difference between ordinary and extraordinary refraction coefficients, Δn, is proportional to square of intensity of applied electric field [4].

The experimental setup consists of He-Ne laser emitting the red light beam of wavelength equal to 632.8 nm, polarizer, two quarter-wave plates and Kerr cell placed between them, analyzer, photodiode, voltmeter that uses the lock-in technique and computer to control measurements and saving measured data.

In order to compute the Kerr constant, the dependence between modulation depth and square of RMS value of modulating voltage applied to the Kerr cell, U_{m}, must be determined. Modulation depth $m_{2\omega}$ is defined by Eq. (1) with use of voltages proportional to light intensity obtained from photodiode. It is equal to the ratio of effective voltage of second harmonic $U_{2\omega}$ to voltage U_{dc} measured by DC voltmeter:

$$m_{2\omega} = \frac{U_{2\omega}}{U_{dc}}. \tag{1}$$

The plot presented in Fig. 2 shows the exemplary dependence of the modulation depth $m_{2\omega}$ on square of modulating voltage U_{m} for OM 10000.
As it can be seen, this dependence is linear, therefore it can be described by simple linear function:

$$m_{2\omega} = aU_m^2 + b. \tag{2}$$

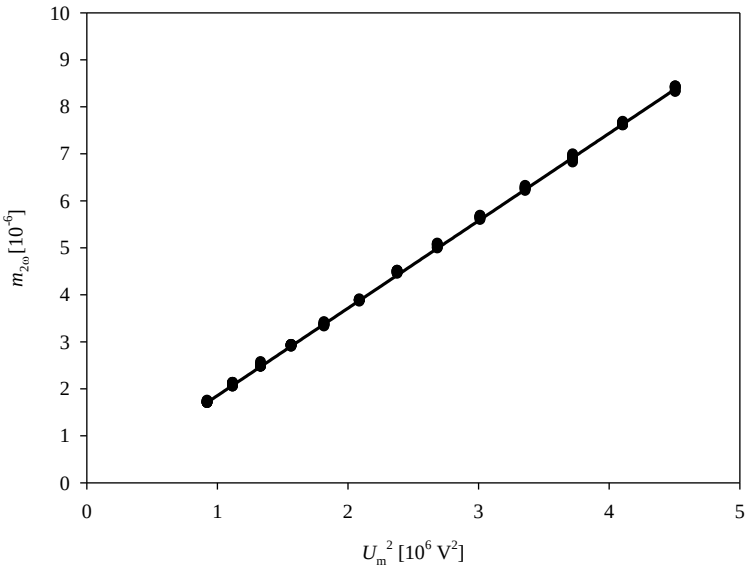

Fig. 2. Modulation depth $m_{2\omega}$ as a function of square of modulating voltage U_m

The slope of the function, a, can be easily determined using least square method. Its magnitude can be also expressed by the function:

$$a = \frac{Kd^2}{\sqrt{2}\pi L} \quad , \tag{3}$$

where d is the distance between electrodes, equal to 4 mm and L is the length of optical path, equal to 99 mm. Thus, the Kerr constant can be calculated from the formula:

$$K = \frac{ad^2}{\sqrt{2}\pi L} \ . \tag{4}$$

The obtained values are shown in Fig. 3 as a function of molecular mass of oils.

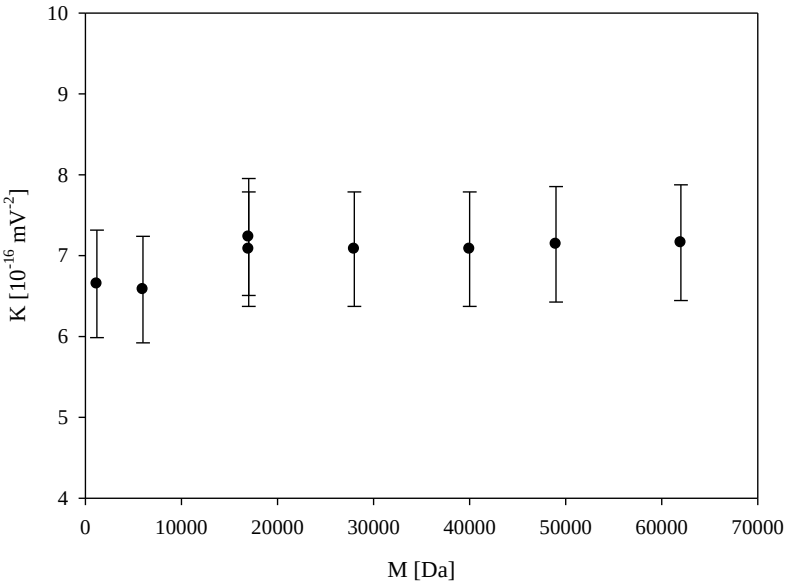

Fig. 3. Dependence between molecular mass of oils on Kerr constant

Having this results, one cannot deduce the character of dependence between Kerr constant and molecular mass of examined oils. The average Kerr constant of methyl silicon oil is equal to $(7.0 \pm 0.7) \cdot 10^{-16}\,\mathrm{mV}^{-2}$.

5. DETERMINATION OF QUADRATIC ELECTROOPTIC COEFFICIENT

Quadratic electro-optic coefficient depends on refractive index [5]. Refractive index of methyl silicon oils was measured by Abbe refractometer. Measurements were performed for oils of different viscosity at temperatures between 280 K and 370 K. Results are presented in Fig. 4 and Fig. 5. They show that viscosity does not have any influence on refractive index. The relationship between refractive index and temperature can be approximated by decreasing linear function.

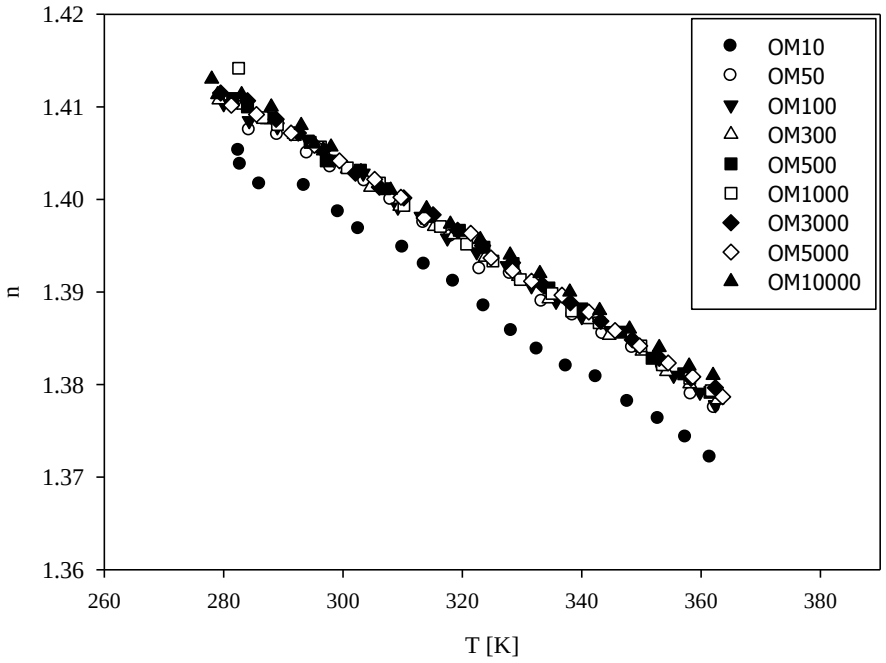

Fig. 4. Temperature dependence of the refractive index for methyl silicon oils for wavelength of light λ = 650 nm

Having the refractive index one can calculate quadratic electro-optic coefficient g_{eff} using the formula:

$$g_{eff} = \frac{2\lambda K}{n^3}. \tag{5}$$

The results for room temperature are shown in Fig. 6.

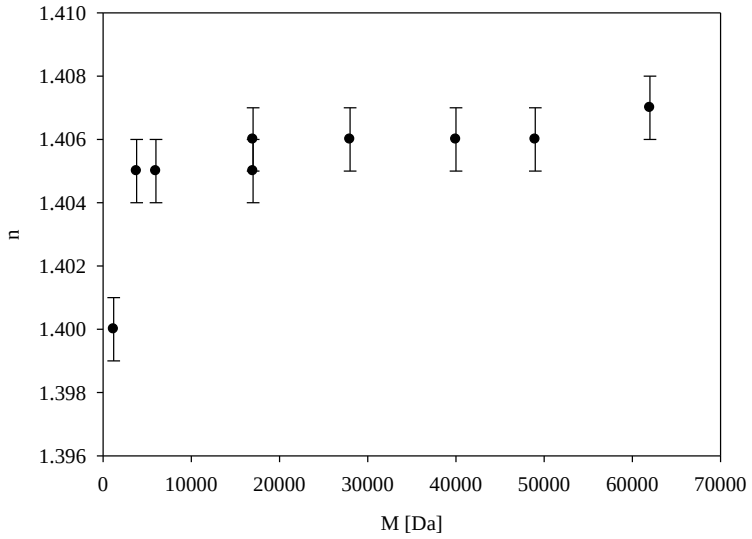

Fig. 5. Dependence of the refractive index on molecular weight for wavelength of light λ = 650 nm at temperature 295 K

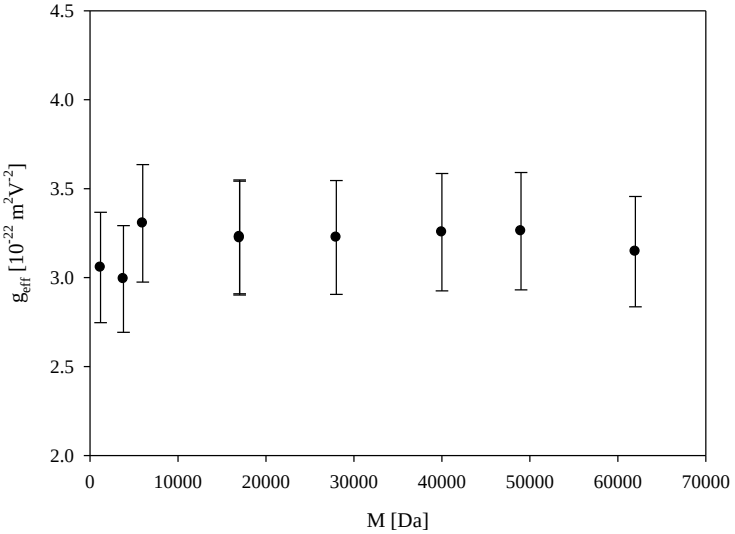

Fig. 6. Dependence of the quadratic electro-optic coefficient on molecular mass of oils

Table 2

Comparison of Kerr constant for different liquids and polymers

	K [10^{-16}mV^{-2}]	ΔK [10^{-16} mV^{-2}]
OM10	6.7	0.7
OM100	6.6	0.7
OM300	7.2	0.7
OM500	7.1	0.7
OM1000	7.1	0.7
OM3000	7.1	0.7
OM5000	7.1	0.7
OM10000	7.21	0.7
Nynas Nytro 10 GBN [6]	18	1
Castor oil – Fresh [7]	151.6	0.7
Castor oil – Aged [7]	141.1	0.6
Fomblin Z [5]	17	1

6. CONCLUSIONS

The obtained results do not let us define character of the dependence between Kerr constant and molecular mass. The Kerr constants have similar values for all tested oils. Similarly, one cannot define character of such dependence for quadratic electro-optic coefficient. Its values depend on Kerr constant and refraction index, which in the given temperature have similar values for all examined oils.

It can be observed that Kerr constant (Fig. 3) as well as quadratic electro-optic coefficient have slightly smaller values for oils of lower molecular mass (OM 50, OM 100).

REFERENCES

[1] **Bielański A.**, Podstawy chemii nieorganicznej, tom 3, PWN, 2002.
[2] Polsil OM – karta katalogowa producenta, Organika Sarzyna SA.
[3] **Marciniak M.**, Wyznaczenie zależności współczynnika załamania światła od temperatury dla wybranych ciekłych polimerów krzemoorganicznych, BSc thesis, Institute of Physics, Lodz University of Technology, 2014.
[4] **Meyer-Arendt J.R.**, Wstęp do optyki, PWN, 1977.
[5] **Ledzion R., Karolczak S., Górski P., Kucharczyk W.**, Sci. Bull. Tech. Univ. Lodz, s. Physics, **29** (2008) 57.

[6] **Kucharczyk W., Ledzion R., Górski P.**, "The effect of aging of transformer oil on the magnitude and temperature dependence of its Kerr constant", Przegląd Elektrotechniczny, (Electrical Rev.), **Vol. 12**, (2014) 40.
[7] **Stępnień M., Ledzion R., Górski P., Kucharczyk W**., Sci. Bull. Tech. Univ. Lodz, s. Physics, **33** (2012) 89.

BADANIE ZALEŻNOŚCI STAŁEJ KERRA I WSPÓŁCZYNNIKA KWADRATOWEGO EFEKTU ELEKTROOPTYCZNEGO W OLEJACH METYLOSYLIKONOWYCH OD ICH MASY CZĄSTECZKOWEJ

Streszczenie

Zbadano zależność stałej Kerra i współczynnika kwadratowego efektu elektrooptycznego od masy cząsteczkowej dla wybranych olejów metylosilikonowych. Na podstawie otrzymanych wyników nie można określić charakteru zależności pomiędzy badanymi wielkościami a masą cząsteczkową.

SCIENTIFIC BULLETIN OF THE LODZ UNIVERSITY OF TECHNOLOGY
No. 1192 Physics, Vol. 35 2014

**KRYSTIAN NOWAKOWSKI, ARTUR PEREK,
MAREK IZDEBSKI, RAFAŁ LEDZION, PIOTR GÓRSKI**

Institute of Physics, Lodz University of Technology
ul. Wólczańska 219, 90-924 Łódź, Poland,
e-mail: izdebski@p.lodz.pl

OPTIMIZATION OF MEASUREMENT CONDITIONS OF KERR CONSTANT IN OPTICALLY ACTIVE LIQUIDS ON THE EXAMPLE OF CASTOR OIL

The results of measurements of Kerr constant in castor oil, obtained by dynamic-polarimetric method are presented. Variable optical path length and four measurement setup configurations were used. They differed by the orientation of polarizer and of quarter-wave plate and therefore they were non-equivalent when other, unwanted effects occurred. It was shown that the Kerr constant measurement performed with use of only one system configuration and one length of optical path may be strongly affected by other effects, however taking the arithmetic mean of two results obtained from appropriate system configurations significantly reduces this error. Theoretical dependences were fitted to the experimental results, which allowed for approximation of other constants, like dichroism, linear birefringence and optical activity induced by external electric field (electrogyration).

Keywords: castor oil, optical polarimetric technique, quadratic electro-optic effect, optical activity, dichroism.

1. INTRODUCTION

Castor oil is a non-edible, light-yellow, transparent and viscous liquid, obtained from the seeds of castor oil plant. It has been used since ancient times in Egypt during mummification and worldwide in traditional medicine [1]. Nowadays it plays an important role in industry, having various applications, including production of paints, food, plastics, medicines, cosmetics, biofuels and many others [1,2]. Its main components are triglycerides of fatty acids, mainly ricinoleic acid (over 89%), linoleic acid (ca. 4%) and oleic acid (ca. 3%) [2]. Although castor oil is considered to be relatively stable, its low oxidative and

temperature stability limits its widespread use. Recently it has been shown, that there is a clear relationship between aging of medical castor oil and its temperature and frequency dependence of the Kerr constant, which is a fact that could be used in continuous quality control systems [3]. However, the cited research on castor oil ageing assumed that it has internal symmetry described by $\infty\infty m$ Curie group, which was later shown to be not the case. In fact, when the oil is enclosed between two, closely spaced, plane-parallel metal electrodes, the internal symmetry is described by $\infty 2$ Curie group [4]. When this lesser symmetry is taken into account, the equations describing Kerr effect and light propagation in castor oil become highly complicated, therefore some assumptions, e.g. lack of dichroism, are usually made to simplify the formulas. Therefore, in order to obtain precise and reliable results, we should carefully consider several other unwanted effects that occur simultaneously during the measurement and may significantly affect the outcome. The effects that should be taken into account are: the natural optical activity [4], the optical activity induced by applied electric field (called the electrogyration effect) [5] and the effects resulting from the interaction of the oil with plane-parallel electrodes immersed in it, such as dichroism and weak linear birefringence with the optical axis perpendicular to the plane of the electrodes [4,6]. The numerical analysis recently presented in Ref. [7] has shown, that the measurement of Kerr effect in castor oil is sensitive to the influence of natural optical activity, linear birefringence, and dichroism, while the electrogyration is less important. According to the numerical simulations performed for medical castor oil, a measurement error is ca. 22% for optical path length of 10 cm. In the same work it was deduced, that there should be two pairs of the possible arrangements of the measurement system, which would result in such errors due to simplifications, that are equal in magnitude, but opposite in sign. Taking the average of these two results would eliminate the error introduced due to simplifications. The aim of this research is to check experimentally the theoretical predictions described above and to formulate practical conclusions concerning the optimal conditions for measuring the Kerr constant.

2. MATHEMATICAL MODEL OF MEASUREMENT

Our earlier observations showed that castor oil between a pair of metal plane-parallel electrodes has an internal symmetry described by $\infty 2$ Curie group with the optical axis directed perpendicularly to the plane of the electrodes [4]. In this situation the only possible form of the vector of applied electric field written in the principal axes system XYZ is $\mathbf{E} = (0, 0, E)$. Let us consider the light beam propagating in the direction $\mathbf{s} = [1, 0, 0]$. The total complex

impermeability tensor [*B*] for this configuration written in the *XYZ* coordinates with the accuracy to the terms proportional to *E* has the following form [7]:

$$[B]=\begin{bmatrix} n_{01}^{-2}+q_{13}E^2 & 0 & 0 \\ 0 & n_{01}^{-2}+q_{13}E^2 & B_{23} \\ 0 & -B_{23} & n_{03}^{-2}+q_{33}E^2 \end{bmatrix}, \tag{1}$$

$$B_{23}=\mathrm{i}\left[n_{01}^{-2}n_{03}^{-2}\left(g_{11}^{(0)}+\beta_{13}E^2\right)+g_{11}^{(0)}\left(n_{01}^{-2}q_{33}+n_{03}^{-2}q_{13}\right)E^2\right], \tag{2}$$

where n_{01} and n_{03} are the principal refractive indices, $g_{ii}^{(0)}$ are the components of natural optical activity tensor, q_{ij} are the components of the quadratic electro-optic tensor, and β_{13} is the component of the quadratic electrogyration tensor (the forms of the tensors can be found, e.g., in Refs. [5,7,8]). It is worth noting that the terms in Eq. (2) containing the products of $g_{11}^{(0)}$ (of the order of 10^{-7}) and q_{ij} are negligible and the term $n_{01}^{-2}n_{03}^{-2}$ is very close to n_0^{-4}, where $n_0 = (n_{01}+n_{03})/2$ is the average refractive index.

Let us introduce another coordinate system, *X'Y'Z'*, related to the experimental setup in which the +*Z'* axis is along the light beam **s'** = [0, 0, 1] and the +*X'* axis defines the reference zero azimuth. A typical experimental setup for measurements of electro-optic coefficients based on the optical polarimetric method consists of a linear polarizer of the azimuth $\alpha_P = \pm 45°$ (relative to +*X'* axis), a cuvette with the oil and immersed electrodes, a quarter-wave plate of the azimuth $\alpha_Q = 0°$ or 90° for the fast wave, and a linear analyzer of any arbitrary azimuth α_A. The intensity *I* of the light passing through this system relative to the intensity I_p behind the polarizer has been derived previously employing Jones calculus [7]:

$$\begin{aligned} \frac{I}{I_p} &= \tfrac{1}{4}\left(T_f^2+T_s^2\right)+ \\ &+\tfrac{1}{4}\left(T_f^2-T_s^2\right)\frac{(B'_{11}-B'_{22})\cos(2\alpha_a)-2z\,\mathrm{Im}[B'_{12}]\sin(2\alpha_A)}{\sqrt{(B'_{11}-B'_{22})^2+4B'_{12}B'^{*}_{12}}}+ \\ &\mp\cos(2\alpha_A)T_fT_s\frac{\mathrm{Im}[B'_{12}]}{\sqrt{(B'_{11}-B'_{22})^2+4B'_{12}B'^{*}_{12}}}\sin\Gamma+ \\ &\mp z\,\tfrac{1}{2}\sin(2\alpha_A)T_fT_s\frac{B'_{11}-B'_{22}}{\sqrt{(B'_{11}-B'_{22})^2+4B'_{12}B'^{*}_{12}}}\sin\Gamma, \end{aligned} \tag{3}$$

where the symbol * indicates the complex conjugate, the upper signs in the "∓" symbol correspond to $\alpha_P = +45°$ and the lower signs to $\alpha_P = -45°$, $z = +1$ for $\alpha_Q = 0°$ and $z = -1$ for 90°, T_f and T_s are the amplitude transmission coefficients for the fast and slow waves, respectively, and Γ is the phase difference between the slow and fast waves

$$\Gamma = \frac{2\pi L}{\lambda}(n_s - n_f)\,. \tag{4}$$

In Eq. (4) λ is the wavelength of the light, L is the light path length between electrodes in the cuvette, and n_f and n_s are the refractive indices of the fast and slow waves, respectively. In the general case, calculation of Γ is a bit more complicated, however, when the relation $B'_{11} + B'_{22} >> \sqrt{(B'_{11} - B'_{22})^2 + 4B'_{12}B'^{*}_{12}}$ is satisfied and n_{01} and n_{03} have very similar values, we can calculate Γ as [5,7]:

$$\Gamma \approx \frac{2\sqrt{2}\,\pi L}{\lambda}\,\frac{\sqrt{(B'_{11} - B'_{22})^2 + 4B'_{12}B'^{*}_{12}}}{(B'_{11} + B'_{22})^{3/2}} \approx \frac{\pi L\, n_0^3}{\lambda}\sqrt{(B'_{11} - B'_{22})^2 + 4B'_{12}B'^{*}_{12}}\,. \tag{5}$$

The matrix of transformation from the *XYZ* to *X'Y'Z'* coordinates can be chosen for example as follows:

$$[\mathbf{a}] = \begin{bmatrix} 0 & 0 & -1 \\ 0 & 1 & 0 \\ 1 & 0 & 0 \end{bmatrix}. \tag{6}$$

Hence, the selected components of the impermeability tensor $[B'] = [\mathbf{a}][B][\mathbf{a}]^T$ written in the *X'Y'Z'* coordinates are:

$$B'_{22} - B'_{11} = n_{01}^{-2} - n_{03}^{-2} + (q_{13} - q_{33})E^2\,, \tag{7}$$

$$B'_{12} = B_{23} \approx \mathrm{i}\, n_0^{-4} g_{11}^{(0)} + \mathrm{i}\, n_0^{-4}\beta_{13}E^2\,. \tag{8}$$

The transmissions T_f and T_s in Eqs. (3) depend on the path length L according to Bouguer's law:

$$T_f^2 = \exp(-\kappa_f L)\,, \quad T_s^2 = \exp(-\kappa_s L)\,, \tag{9}$$

where κ_f and κ_s [1/m] are the length-independent absorption coefficients. The difference $\kappa_f - \kappa_s$ is related with the relative difference D in transmissions:

$$D(L) = (T_f - T_s)/\overline{T} = 2\tanh\left[-0.25(\kappa_f - \kappa_s)L\right], \tag{10}$$

where $\overline{T} = (T_f + T_s)/2$ is the average transmission coefficient. The relationship (10) allows to calculate $D(L)$ for any path length L when the value of D is given for any fixed length. The other expressions in Eq. (3), which depend on the transmission coefficients, can be calculated as follows:

$$T_{\mathrm{f}}^2 + T_{\mathrm{s}}^2 = 2\overline{T}^2\left(1+0.25D^2\right), \tag{11}$$

$$T_{\mathrm{f}}^2 - T_{\mathrm{s}}^2 = 2\overline{T}^2 D^2, \tag{12}$$

$$T_{\mathrm{f}} T_{\mathrm{s}} = \overline{T}^2\left(1-0.25D^2\right). \tag{13}$$

Since all the expressions in Eq. (3) are proportional to $\overline{T}^2$ this variable reduces in calculations of modulation index related to the changes in the intensity I due to an applied electric field E.

3. EXPERIMENTAL

3.1. Method

The dynamic-polarized method is based on measuring the intensity of light passing through Kerr cell placed between crossed polarizers. Across the Kerr cell, a sinusoidal alternating electric field of frequency 417 Hz was applied. As the Kerr effect depends here on the square of the electric field, the change in optical properties of the medium was modulated with the frequency equal to the second harmonics of the field frequency, since the Kerr effect is the same for both directions of the field. Two components of the emerging light were measured, the constant component I_0 and the component at the second harmonics of the modulating field $I_{2\omega}$. Calculating the ratio of these two quantities, we get modulation index $m_{2\omega}$ defined as $m_{2\omega} = I_{2\omega} / I_0$. Since we were using a photodiode to measure light intensity, it is also possible to express $m_{2\omega}$ as a function of the amplitudes of signals given by the photodiode, rather than light intensities:

$$m_{2\omega} = \frac{I_{2\omega}}{I_0} = \frac{U_{2\omega}}{U_0}, \tag{14}$$

where $U_{2\omega}$ is the RMS voltage of the signal from photodiode at the second harmonics of the applied field frequency and U_0 is the constant component of the signal from photodiode. To the best of our knowledge, all the previous research in this matter assumed that the modulation index $m_{2\omega}$ is a linear function of the square of applied voltage (or electric field), i.e.:

$$m_{2\omega} = a\,U_{\mathrm{m}}^2 + b, \tag{15}$$

where U_{m} is the RMS voltage applied to the electrodes and a is the slope. This assumption holds true if the simplifications mentioned in the introduction are valid. If this relation is indeed linear, then it is possible to calculate the Kerr coefficient K of the material using the following formula:

$$K = \frac{a\,d^2}{\sqrt{2}\,\pi L}, \tag{16}$$

where d is the distance between the electrodes and L is the optical path length.

3.2. Setup

The Kerr cell was a glass cuvette with stainless steel electrodes immersed in castor oil. A separator made of polycarbonate fixed electrodes in positions. The cross-section of this setup is presented in Fig. 1.

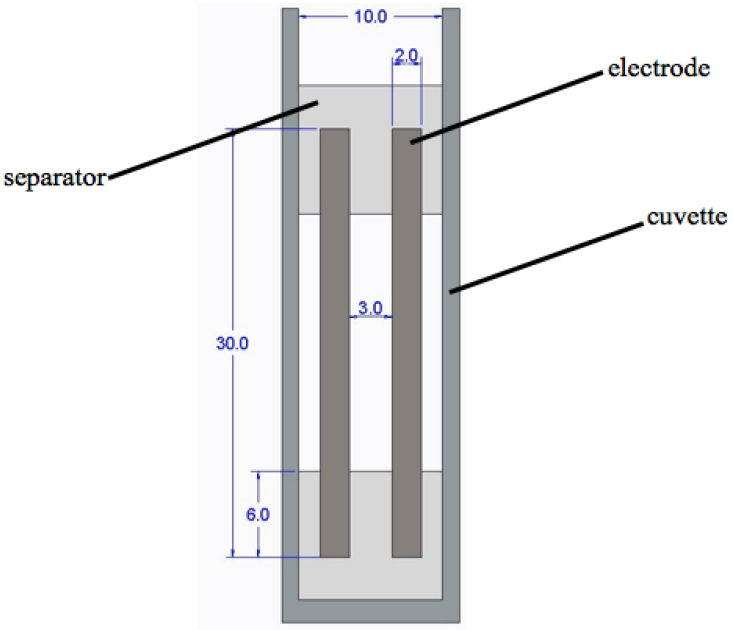

Fig. 1. Cross-section of the experimental Kerr cell

The length of electrodes was 99 ± 0.1 mm and 49 ± 0.1 mm. The light beam was directed perpendicularly to the applied electric field. The distance d between the electrodes was 3 ± 0.02 mm. The optical path length was increased by adding more cuvettes and connecting electrodes in series, with the step of 4.9 cm. Thus, there was 2 mm of glass between adjacent electrodes, as the cuvettes' walls are 1 mm thick. Nevertheless this system was assumed to be one uniform Kerr cell of greater length. The oil under investigation was Sigma-Aldrich castor oil number 259853 (batch number MKBL5196). The oil was poured into cuvettes

10 days before the first measurement, to allow little air bubbles to escape, as castor oil is dense and highly viscous. The measurements were carried out for another 13 days, so altogether the oil spent 23 days in cuvettes, all the time open to air and in stable temperature of 20-22°C. The complete measurement system is presented schematically in Fig. 2.

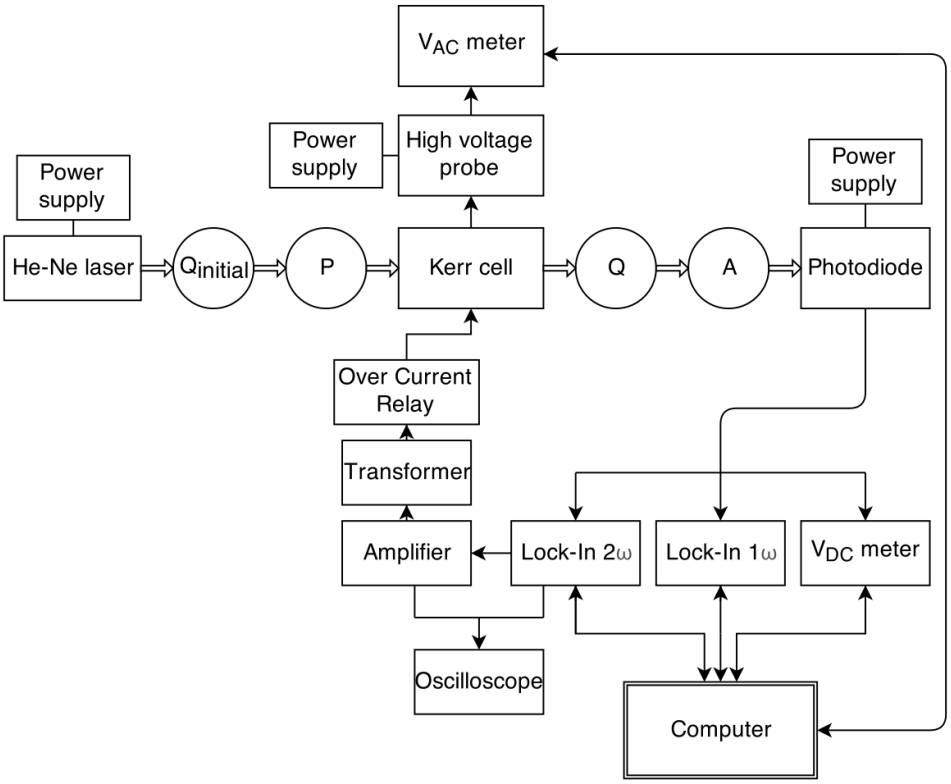

Fig. 2. Scheme of the measurement system

The light source was a He-Ne laser of wavelength $\lambda = 632.8$ nm. Letters Q, P and A stand for quarter-wave plate, polarizer and analyzer, respectively. An additional $Q_{initial}$ quarter-wave plate placed between the laser and the polarizer was oriented in such a way that it changed the polarization of light to circular. The RMS of voltage applied to the electrodes in the Kerr cell was measured by Keithley multimeter 2000 through Tektronix P6015 high voltage probe. The intensity of light behind the analyzer was measured by Thorlabs photodiode PDA100A-EC. Three components of that signal were recorded. The DC

component was measured by Keithley multimeter 2700, the RMS of components at the first and at the second harmonic of modulating field were measured by digital signal processing lock-in amplifiers produced by EG&G instruments, model 7265. One of the lock-in amplifiers was also used for generating the modulating signal, that was later amplified and passed through a transformer in order to obtain voltages up to 3 kV. An over-current relay was added after the transformer for safety. A computer program controlled the measurement process and data acquisition.

3.3. Procedure

According to the theoretical analysis in Ref. [7], the settings giving desired series of results, that have errors equal in magnitude but opposite in sign, differ from each other only by the rotation of quarter-wave plate *Q* by 90°. Turning the polarizer *P* by 90° allows to obtain a different pair of series. The reference direction, that we will use to describe the orientation of optical elements, is the normal to the electrode surfaces. The angle 0° means direction perpendicular to the electrode surfaces and angle 90° means direction tangent to these surfaces. The orientation of the optical axis of the analyzer *A* was constant throughout the experiment, and equal to −45°. Shorthand notation of this orientation will be $\alpha_A = -45°$. The polarizer and quarter-wave plate orientation will be described in the same way as α_P and α_Q. When it comes to the quarter-wave plate *Q*, its position will be described by two arbitrary numbers, −1 and 1. One of them means that the extraordinary axis is perpendicular to the electrode surfaces and the other means that it is parallel to them. We have no way to recognize which one is which; nevertheless, the measurement was done for both orientations. The experimental procedure was as follows:

1. Set $\alpha_A = -45°$ and $\alpha_P = 45°$ (polarizer and analyzer crossed).
2. Insert the first Kerr cell of length 4.9 cm to the system.
3. Set $\alpha_Q = 1$.
4. Measure the Kerr effect for a given voltage range.
5. Turn *Q* by 90°, i.e. set $\alpha_Q = -1$.
6. Measure the Kerr effect for a given voltage range again.
7. Increase the length of the Kerr cell by inserting next cuvette.
8. Repeat steps 3-7 until achieving the maximal length (L = 79.2 cm).
9. Set $\alpha_P = -45°$ (optical axes of polarizer and analyzer are parallel).
10. Repeat steps 3-7, this time decreasing the path length by removing cuvettes.

The voltages applied to the electrodes were not exactly the same for every path length, as adding more cuvettes increased the capacitance of the system, resulting in lower field strength across the Kerr cell for the same signal generated by Lock-in amplifier. The program took 10 measurements at each voltage value, in the range of ca. 350-2000 V, with the step of ca. 70 V.

4. RESULTS

First of all, according to Eq. (14), the modulation index $m_{2\omega}$ was calculated and then plotted against the square of the RMS of voltage applied to the electrodes, U_{m}^2. Then a linear function was fitted to the data points and its slope *a*, needed to calculate the Kerr constant according to Eq. (16), was get. Some exemplary results are plotted in Fig. 3, for easier comparison, for $m_{2\omega}/L$ as a function of the square of the electric field intensity E^2.

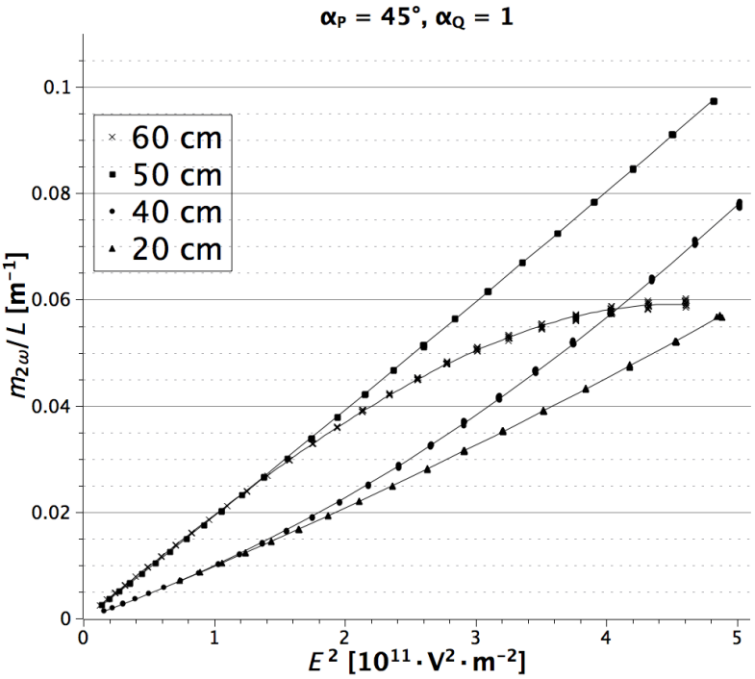

Fig. 3. The experimental dependence of the ratio of modulation index to path length, $m_{2\omega}/L$, on the square of electric field intensity E^2 for SIGMA ALDRICH castor oil at room temperature and field frequency 417 Hz for crossed polarizer and analyzer

As it can be seen, not only are the relationships non-linear, but also they tend to change their general shape, e.g. the curve for 40 cm is parabolic, curve for 50 cm becomes more linear again, while the curve 60 cm has exponential-like shape. Because of this nonlinearity, Eq. (16) was not used to find the Kerr constant K for the optical path lengths over 50 cm. For the same reason, only the linear part of the above plot was used for fitting for L = 40 cm. The values of Kerr constant K, obtained from Eq. (16), are plotted below, as a function of L:

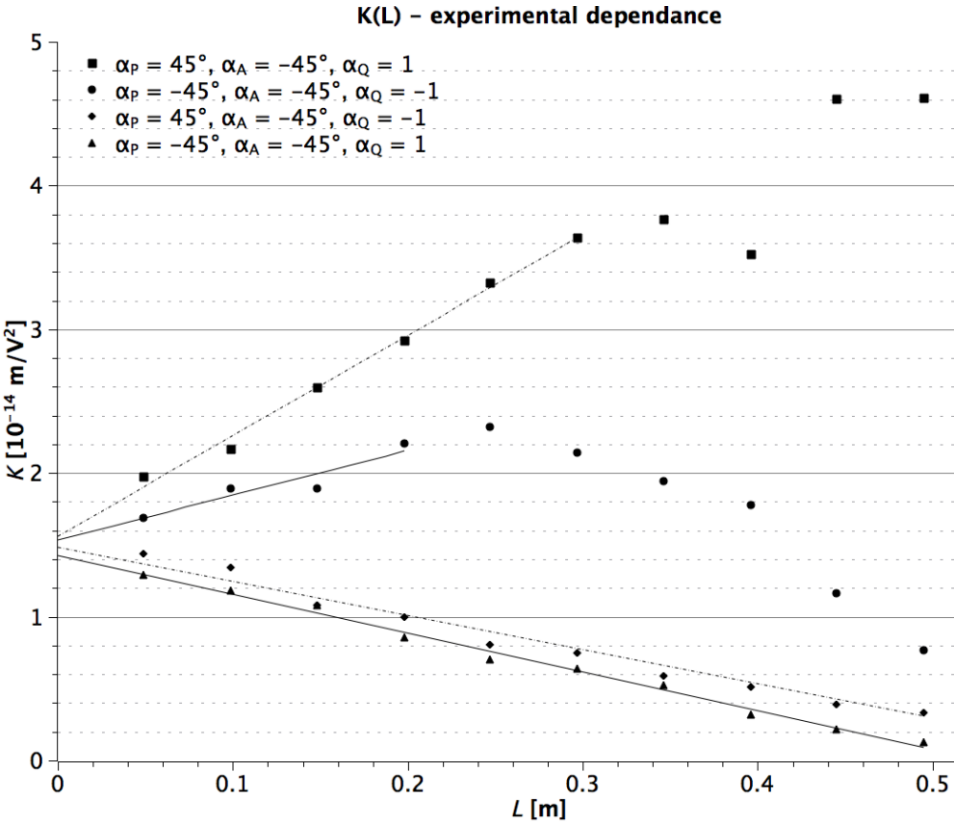

Fig. 4. The experimental dependences of the Kerr constant K on the path length L obtained for SIGMA-ALDRICH castor oil at room temperature and frequency 417 Hz for the four combinations of the polarizer and quarter-wave azimuths

The experimental dependence of K on L was used to match the constants $n_{01} - n_{03}$, β_{13}, and $(T_f - T_s)/\overline{T}$ for L = 10 cm, which are present in the theoretical

relationships given in Chapter 2. Furthermore, we used the following fixed constants, which are known in advance from various measurements:

- $n_0 = 1.48$ [5],
- the Kerr constant $K = 1.5 \cdot 10^{-14}$ mV^{-2} obtained in this work by extrapolating the experimental $K(L)$ dependences for $L \to 0$, which allows to calculate the effective coefficient of the quadratic electro-optic effect $|q_{33} - q_{13}| = 2\lambda K/n_0^3 \approx 5.8 \cdot 10^{-21}$ m^{2}V^{-2},
- the angle $\phi = -3.5°$ of turning of the polarization plane in the oil obtained in this work for $L = 10$ cm and $\alpha_P = 0$, which allows to calculate $g_{11}^{(0)} = -1.82 \cdot 10^{-7}$ according to the formula $g_{11}^{(0)} = \lambda n_0 \phi/(\pi L)$ derived in Ref. [5].

The lock-in amplifier was simulated numerically by computing the coefficients in the following Fourier series:

$$\frac{I}{I_\mathrm{p}} = \frac{I_0}{I_\mathrm{p}} + \frac{I_\omega}{I_\mathrm{p}} \sin(\omega t + \varphi_1) + \frac{I_{2\omega}}{I_\mathrm{p}} \sin(2\omega t + \varphi_2) + \ldots , \tag{17}$$

for I/I_p given by Eq. (3) with substituted equations (5), (7), (8) and (10)-(13). Then, the coefficients of this series were used to calculate the modulation index:

$$m_{2\omega} = \frac{I_{2\omega}/I_\mathrm{p}}{I_0/I_\mathrm{p}} . \tag{18}$$

Since the dependence of $m_{2\omega}$ on U_m^2 may differ from the linear function in Eq. (15), our calculations were performed for various U_m voltages and the average slope a was matched. Then, the Kerr constant was calculated like for the experimental data, employing Eq. (16).

The numerically obtained $K(L)$ dependences shown in Fig. 5 are roughly in line with all four experimental series in Fig. 4 when the following constants are substituted:

$$\left|T_\mathrm{f} - T_\mathrm{s}\right| / \overline{T} = 0.034 \quad \text{for the path length } L = 0.1 \text{ m}, \tag{19}$$

$$|n_{01} - n_{03}| = 2.5 \cdot 10^{-7}, \tag{20}$$

$$|\beta_{13}| = 1.0 \cdot 10^{-20} \text{ m}^2\text{V}^{-2}. \tag{21}$$

Although the signs of $T_\mathrm{f} - T_\mathrm{s}$, $n_{01} - n_{03}$, β_{13} and $q_{33} - q_{13}$ can not be completely arbitrary, some combinations of the signs lead to similar results and we can not unambiguously determine the signs of individual constants.

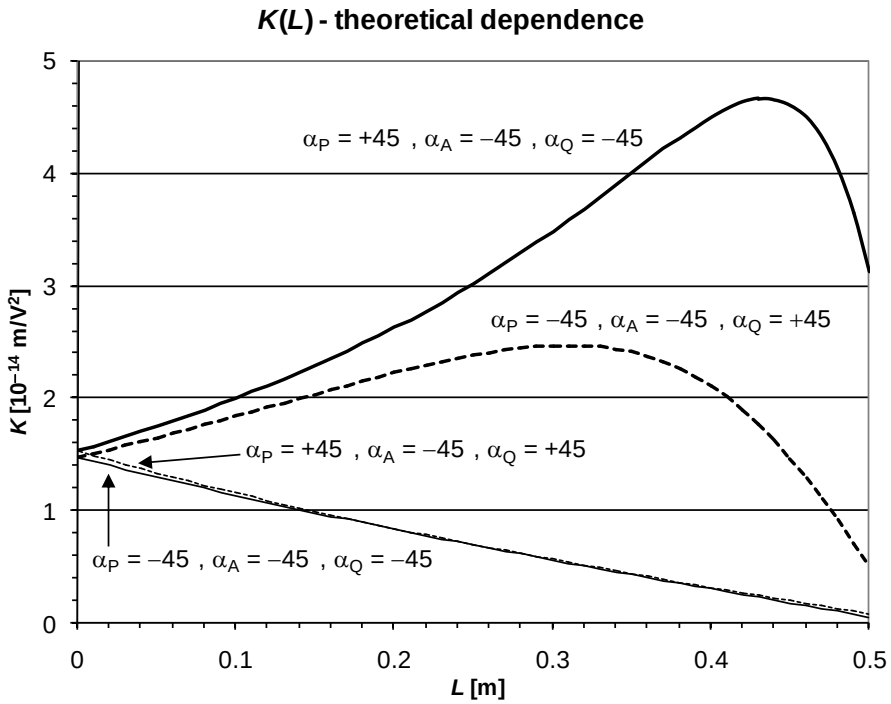

Fig. 5. The theoretical dependences of the Kerr constant K on the path length L obtained for $(T_f - T_s)/T = -0.034$ for path length 0.1 m, $n_{01} - n_{03} = 2.5 \cdot 10^{-7}$, $q_{33} - q_{13} = 5.8 \cdot 10^{-21}$ m^{2}V^{-2} and $\beta_{13} = -1.0 \cdot 10^{-20}$ m^{2}V^{-2}

It is worth noting that to obtain a satisfactory agreement between the theoretical and experimental dependences, we cannot neglect any of the effects such as the linear birefringence, the dichroism, the natural optical activity and the quadratic electrogyration effect.

5. CONCLUSIONS

Our experimental results obtained for pure castor oil for research purposes confirm the existence of the effects observed previously in other experimental systems, such as the linear birefringence [4,6], the dichroism [4,6], the natural optical activity [4], and the optical activity induced by an applied electric field (electrogyration effect) [5], which are not taken into account in the simplified formula (16) typically applied to processing of experimental data. It is possible to derive the exact formula, which takes into account all of the phenomena mentioned. However, in practice the use of such formula would be very

problematic because of its complexity and dependence on a number of coefficients that require measurements in other experimental setups. Moreover, some of these coefficients are likely to be unstable and sensitive to many factors such as the oil purity, ageing processes, temperature, the history of the applied electric field including many hours before the measurement and others. In this situation, our goal is to find such a way of determining the Kerr constant that allows for reducing the influence of unwanted effects, so it is not necessary to measure them beforehand.

Our new experimental results and numerical analysis confirms the conclusion reached previously in Ref. [7] that the contribution of undesirable effects can be substantially reduced by calculating the arithmetic mean of the two values of Kerr constant calculated according to the formula (16) for the two measurements differing in the orientation of the quarter-wave plate. However, this conclusion requires the addition of a new assumption that these two measurements should be carried out for a parallel orientation of the analyzer to polarizer. The measurements performed in traditional configuration with crossed polarizers and various orientations of quarter-wave plate do not ensure as good reduction of errors in the arithmetic mean.

The values of the linear birefringence and dichroism estimated in this work are in good agreement with the results obtained previously for medical castor oil [4]. The value of the dichroism $|T_\mathrm{f} - T_\mathrm{s}|/\overline{T} = 1.0 \cdot 10^{-2}$ (for L = 10 cm) obtained recently in Ref. [5] is significantly smaller, but this results probably from instability of this coefficient rather than from erroneous measurement method.

The absolute value of the electrogyration coefficient $|\beta_{13}| = 1.0 \cdot 10^{-20}$ m^{2}V^{-2} estimated roughly in this work is much higher than the value $1.4 \cdot 10^{-22}$ m^{2}V^{-2} obtained previously in another measurement system [5]. According to our best knowledge there are no other published results for liquids, and we can only conclude that both values are in the range of values $10^{-22} \ldots 10^{-18}$ known from the literature for solid crystals at room temperature [9]. At the present stage of research we cannot decide whether one of the results is erroneous, because it is possible that we are dealing with a coefficient that is unstable.

REFERENCES

[1] **Khan I.A., Abourashed E.A.,** Leung's Encyclopedia of Common Natural Ingredients Used in Food, Drugs and Cosmetics, John Wiley & Sons, Inc., 2010.

[2] **Ogunniyi D.S.,** Bioresource Technology **97(9)** (2006) 1086.

[3] **Stępień M., Ledzion R., Górski P., Kucharczyk W.,** Sci. Bull. Lodz Univ. Tech., s. Physics, **33** (2012) 89.

[4] **Izdebski M., Ledzion R., Górski P.,** Sci. Bull. Lodz Univ. Tech., s. Physics, **33** (2012) 39.
[5] **Izdebski M., Ledzion R., Górski P.,** "Measurement of quadratic electrogyration effect in castor oil", in review in Optics Communications.
[6] **Izdebski M., Ledzion R.,** "New method for measurement of very weak linear birefringence and dichroism in liquids on the example of castor oil between metal electrodes", this volume.
[7] **Izdebski M., Ledzion R., Kucharczyk W.,** Sci. Bull. Lodz Univ. Tech., s. Physics, **34** (2013) 5.
[8] **Sirotin Yu.I., Shaskolskaya M.P.,** Fundamentals of crystal physics, Mir Publishers, 1982.
[9] **Bhalla A.S., Cook W.R., Hearmon R.F.S., Jerphagnon J., Kurtz S.K., Liu S.T., Nelson D.F., Oudar J.-L.,** Crystal and solid state physics, in: Hellwege K.-H., Hellwege A. (Eds.), Landolt-Börnstein Numerical Data and Functional Relationships in Science and Technology, **Vol. 18** of New Series, Group III, Springer, Berlin, 1984, pp. 431-434.

OPTYMALIZACJA WARUNKÓW POMIARU STAŁEJ KERRA W CIECZACH AKTYWNYCH OPTYCZNIE NA PRZYKŁADZIE OLEJU RYCYNOWEGO

Streszczenie

Przedstawiono wyniki pomiarów stałej Kerra w oleju rycynowym metodą polaryzacyjno-optyczną dla różnych długości drogi światła w próbce przy czterech konfiguracjach pomiarowych, nierównoważnych pod względem wpływu innych niepożądanych efektów, które różnią się orientacjami polaryzatora i płytki ćwierćfalowej. Pokazano, że pomiar stałej Kerra przeprowadzony dla tylko jednej konfiguracji pomiarowej przy jednej długości drogi światła w próbce może być obciążony znacznym wkładem kilku innych niepożądanych efektów, jednakże obliczenie średniej arytmetycznej z pomiarów w dwóch odpowiednio dobranych konfiguracjach pomiarowych pozwala na znaczne zredukowanie błędów pomiarowych. Do wyników doświadczalnych dopasowano zależności teoretyczne, co oprócz pomiaru stałej Kerra pozwoliło także na zgrubne oszacowanie innych wielkości takich jak dichroizm, liniowa dwójłomność i aktywność optyczna indukowana polem elektrycznym (elektrożyracja).

SCIENTIFIC BULLETIN OF THE LODZ UNIVERSITY OF TECHNOLOGY
No. 1192 Physics, Vol. 35 2014

ARTUR PEREK, RAFAŁ LEDZION, MAREK IZDEBSKI, KRYSTIAN NOWAKOWSKI, PIOTR GÓRSKI

Institute of Physics, Lodz University of Technology
ul. Wólczańska 219, 90-924 Łódź, Poland
e-mail: rafal.ledzion@p.lodz.pl

INFLUENCE OF ELECTRODE MATERIAL AND SPACING BETWEEN ELECTRODES ON MEASUREMENT OF KERR CONSTANT IN CASTOR OIL

The influence of the electrode material and of the spacing between electrodes on Kerr constant in castor oil is investigated. It is shown that the spacing of the electrodes influences the measurement of Kerr constant whereas the electrode material has no influence on the results of the measurement.

Keywords: castor oil, electrode material, electro-optic effect, Kerr constant.

1. INTRODUCTION

Kerr effect is a change of refractive index of a medium induced by electric field. The effect is directly proportional to the square of the applied electric field. The change in indices of refraction differs for polarizations of light parallel and perpendicular with respect to the applied field. Such optically anisotropic medium is called birefringent. The birefringence defined as the difference Δn between refractive indices is given by the formula:

$$\Delta n = \lambda K E^2, \tag{1}$$

where λ is the wavelength of light, K is Kerr constant and E is the electric field strength.

Castor oil is a nearly transparent yellow liquid obtained from seeds of *Ricinus communis* plant and its main component is ricinoleic acid [1]. Applications for castor oil range from personal care products through industrial materials up to component of biodiesel [2], and biodegradable foam plastics [3]. Research shows [4] that the electro-optic Kerr effect can be used to estimate the ageing processes in castor oil and probably in other oils of natural origin. Our previous work [5] shows that birefringence and dichroism arise between parallel plate electrodes made of stainless steel without electric field applied. Both effects might significantly influence the measurement of Kerr constant [6]. However no investigations were conducted concerning influence of electrode material and their separation on measurement of Kerr constant in castor oil.

The aim of this work is to investigate whether the electrode material, namely stainless steel, aluminum and copper, influences the measurement of Kerr constant in castor oil and also to study the dependence of Kerr constant on the electrodes spacing.

2. EXPERIMENTAL

Dynamic polarimetric method [7] was used to measure the Kerr constant. The method is based on harmonic analysis of the intensity of light passing through the Kerr cell placed between crossed polarizer and analyzer. The intensity of emerging light beam from such a system is given by following equation [8]:

$$I = I_0\left\{\cos^2(\alpha) - \sin(2\rho)\sin[2(\rho-\alpha)]\sin^2\left(\frac{\Gamma}{2}\right)\right\} . \tag{2}$$

The incident light intensity is denoted by I_0, α is the angle between the planes of polarization in the polarizer and analyzer, ρ stands for the angle between the plane of polarization in the polarizer and direction of the applied electric field. The phase difference Γ between ordinary and extraordinary beams is given by the formula:

$$\Gamma = \Gamma_0 + kL\Delta n, \tag{3}$$

where Γ_0 is phase difference independent of the electric field, $k = 2\pi/\lambda$, L is electrode length and Δn stands for birefringence induced by electric field. When crossed polarizers are oriented so that $\rho = \pi/4$ and the phase difference introduced by quarter wave plate $\Gamma_0 = (2m + 1)\pi/2$ where m is a natural number, then Eq. (2) simplifies to the following form:

$$I = \frac{I_0}{2}\left[1 + \sin\left(kL\Delta n\right)\right]. \tag{4}$$

For sinusoidal modulating voltage, the Kerr constant may be expressed as:

$$K = \frac{ad^2}{\sqrt{2}\pi L}, \tag{5}$$

where d is the spacing between electrodes, a is slope in the simple linear regression of modulation index $m_{2\omega}$:

$$m_{2\omega} = \frac{U_{2\omega}}{U_{dc}} \tag{6}$$

expressed as a function of square of the modulating voltage U_m:

$$m_{2\omega} = aU_m^2 + b. \tag{7}$$

$U_{2\omega}$ is the RMS value of the voltage measured at second harmonic of the light transmitted through the system of which constant component is proportional to U_{dc} voltage measured. The error ΔK was calculated using exact differential method which gives the formula:

$$\Delta K = \frac{d^2}{\sqrt{2}\pi L}\Delta a + \frac{2ad}{\sqrt{2}\pi L}\Delta d + \frac{ad^2}{\sqrt{2}\pi L^2}\Delta L. \tag{8}$$

The analysis of error indicates that over 90% of ΔK corresponds to the second term of Eq. (8). For the purpose of this experiment, three sets of plane-parallel electrodes were polished to minimize surface contamination and sharp edges. The electrodes were placed in the glass cuvette and filled with analytical grade castor oil produced by Sigma-Aldrich designated by catalog number 259853 and batch number MKBL5196. Each pair of the electrodes of length equal to 99 mm was separated by five separators providing 3 mm gap between the electrodes. The theoretical analysis of measurement of quadratic electro-optic effect in castor oil [6] predicts that for two positions of quarter-wave plate, P_1 and P_2, differing by the angle $\pi/2$, the systematic error increases the result for one position of quarter wave plate and decreases it, by the same percent, for the other position. The systematic error was eliminated by measurement of K in both positions and averaging the results.

The experiment was performed in three phases. First, each electrode material was used to measure Kerr constant using sinusoidal modulating voltage of 417 Hz frequency. The second part of the experiment was the measurement

of Kerr constant using modulating voltage frequencies ranging from 117 Hz up to 5017 Hz. Third part of the experiment was performed using copper electrodes with spacing ranging from 2.1 mm to 8.3 mm. For the purpose of this experiment, the ranges of applied modulating voltage corresponded to the same range of applied electric field. Whole experiment was performed employing He-Ne laser of wavelength $\lambda = 633$ nm. The RMS value of modulating voltage U_m was within range from 200 V to 3000 V. The measurements were performed using lock-in technique and computer controlled data acquisition system.

3. RESULTS

The first part of measurements was performed at temperature 295 K using modulating voltage frequency 417 Hz. Figure 1 presents results of the measurements for stainless steel, copper and aluminum electrodes. The average results for each material are gathered in Table 1.

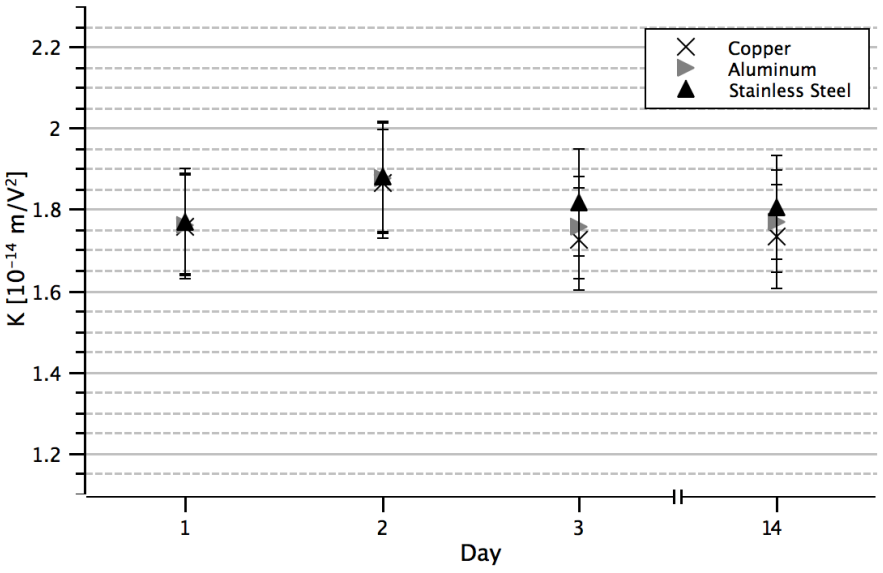

Fig. 1. The average values of Kerr constant for two equivalent positions of the quarter wave plate differing by $\pi/2$ with corresponding error $\Delta K = 0.13 \cdot 10^{-14} \mathrm{m/V^2}$

Table 1

The average results for each material; first part of measurements, $\Delta K = 0.13 \cdot 10^{-14}\text{m/V}^2$

Day	Copper $K\,[10^{-14}\text{m/V}^2]$	Aluminum $K\,[10^{-14}\text{m/V}^2]$	Stainless Steel $K\,[10^{-14}\text{m/V}^2]$
1	1.76	1.76	1.77
2	1.86	1.88	1.88
3	1.73	1.76	1.82
4	1.73	1.77	1.80
average	1.77	1.79	1.82

The results of the second part of the measurements, performed with use of various modulating voltage frequencies, are presented in Figure. 2 and in Table 2 with measurement error $\Delta K = 0.13 \cdot 10^{-14}\text{m/V}^2$.

Table 2

The average results for each material; second part of measurements $\Delta K = 0.13 \cdot 10^{-14}\text{m/V}^2$

ω[Hz]	Copper $K\,[10^{-14}\text{m/V}^2]$	Aluminum $K\,[10^{-14}\text{m/V}^2]$	Stainless Steel $K\,[10^{-14}\text{m/V}^2]$
117	1.72	1.75	1.81
217	1.74	1.76	1.82
317	1.73	1.76	1.82
417	1.72	1.76	1.80
517	1.72	1.74	1.78
617	1.72	1.73	1.77
817	1.71	1.73	1.75
1017	1.71	1.73	1.77
1517	1.72	1.75	1.78
2017	1.73	1.76	1.79
2517	1.74	1.77	1.78
3017	1.78	1.81	1.83
3517	1.74	1.77	1.79
4017	1.71	1.74	1.75
5017	1.70	1.76	1.77

The results of the third part of the experiment presented in Fig. 3 and Table 3 are related to the dependence of Kerr constant on electrode spacing for positions P_1 and P_2 of quarter wave plate differing by $\pi/2$. Copper electrodes with spacing 2.1 mm, 3.0 mm, 4.0 mm, 6.2 mm and 8.3 mm were used. The ranges of modulating voltage U_m corresponds to the same range of applied electric field, namely from 90 kV/m to 350 kV/m.

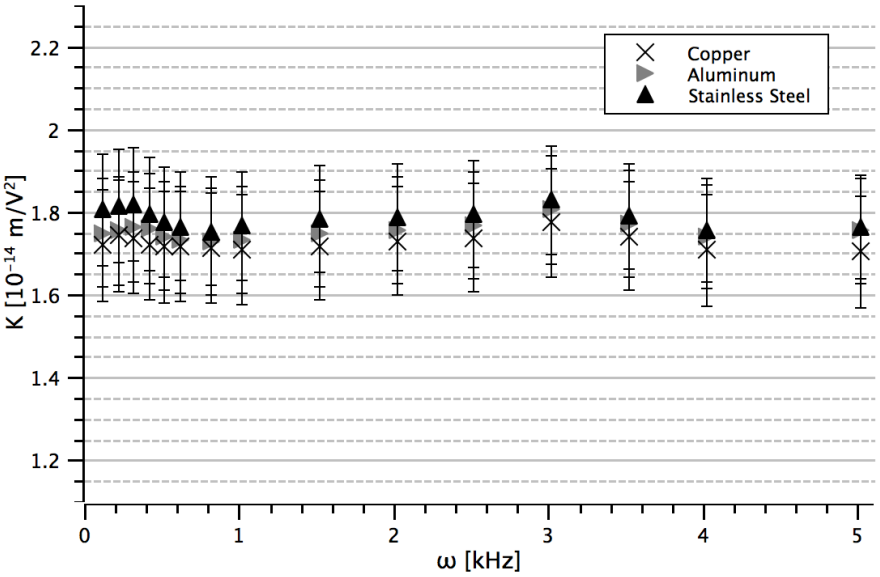

Fig. 2. The dependence of Kerr constant on frequency for different electrode materials

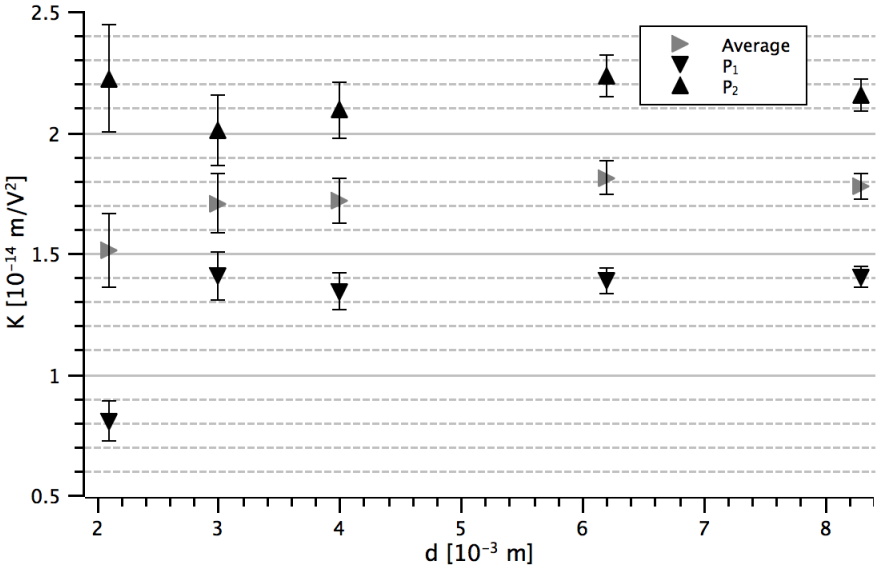

Fig. 3. The dependence of Kerr constant on electrode spacing for positions P_1 and P_2 and their average

Table 3

The Kerr constant dependence on spacing between electrodes

Distance d [mm]	Position 1 $K\,[10^{-14}\,\mathrm{m/V^2}]$	Position 2 $K\,[10^{-14}\,\mathrm{m/V^2}]$	Average $K\,[10^{-14}\,\mathrm{m/V^2}]$
2.1	0.81 ± 0.08	2.22 ± 0.22	1.52 ± 0.15
3	1.41 ± 0.10	2.01 ± 0.15	1.71 ± 0.12
4	1.34 ± 0.07	2.10 ± 0.12	1.71 ± 0.10
6.2	1.39 ± 0.05	2.24 ± 0.09	1.81 ± 0.07
8.3	1.40 ± 0.04	2.15 ± 0.07	1.78 ± 0.06

4. CONCLUSIONS

The results obtained during the first part of experiment indicate that examined electrode materials, namely copper, aluminum and stainless steel, had no influence on Kerr constant during 14 days of measurements or their influence is smaller than the measurement error. The second part of the experiment indicates that stainless steel might increase Kerr constant over broad spectrum of frequencies, however the temperature log shows that copper and aluminum were measured at temperature 295 K along with every other measurement except stainless steel which was measured at 292 K during this part. According to [4], the decrease in temperature by 3 K would increase Kerr constant by $0.07 \cdot 10^{-14}\,\mathrm{m/V^2}$. In fact, similar differences are observed in Table 2. Such susceptibility of Kerr constant to changes of temperature suggests a need for temperature control. The third part of experiment demonstrates the influence of distance of electrodes on Kerr constant. The castor oil in a sufficiently high volumes is an non-dichroic isotropic liquid of $\infty\infty$ symmetry. However, previous research [5] shows that the same oil placed between plane-parallel electrodes becomes dichroic and anisotropic with the optical axis perpendicular to the plane of electrodes, even when the spacing between electrodes is in the order of millimeters. The linear birefringence and dichroism arise between electrodes even without electric field applied. This indicates that the electrodes cause the transition of the oil symmetry from $\infty\infty$ to $\infty 2$ Curie group, which is associated with a change in the form of the tensor of the quadratic electro-optic effect (the tensor is given, e.g., in Ref. [6]). Additionally recent research [9] and [10] also demonstrate linear birefringence $n_{01} - n_{03}$ arising between plane-parallel electrodes. Therefore the dependence presented in third part of the experiment might be caused by orientational ordering of ricinoleic acid molecules induced by narrow gap between electrodes. Knowledge about induced orientation of oil molecules might be crucial when the molecules are oriented by electric field,

such induced orientation might influence Curie group describing internal symmetry of the oil [5].

REFERENCES

[1] **Achaya K.T., Craing B.M., Youngs C.G.**, J. Am. Oil Chem. Soc., **41** (1964) 783.
[2] **Deshpande D.P., Urunkar Y.D., Thakare P.D.**, Res. J. Chem. Sci., **2** (2012) 51.
[3] **Wang W.J., Rong M.Z., Zhang M.Q., Hu J., Chen H.W., Czigány T.**, Biomacromolecules, **9** (2008) 615.
[4] **Stępień M., Ledzion R., Górski P., Kucharczyk W.**, Sci. Bull. Lodz Univ. Tech., s. Physics, **33** (2012) 89.
[5] **Izdebski M., Ledzion R., Górski P.**, Sci. Bull. Lodz Univ. Tech., s. Physics, **33** (2012) 39.
[6] **Izdebski M., Ledzion R., Kucharczyk W.**, Sci. Bull. Lodz Univ. Tech., s. Physics, **34** (2013) 5.
[7] **Ledzion R., Bondarczuk K., Górski P., Kucharczyk W.**, Cryst. Res. Technol., **34** (1999) 745.
[8] **Born M., Wolf E.**, Principles of Optics, Cambridge Univ. Press, Cambridge, 2005, p. 825.
[9] **Izdebski M., Ledzion R.,** Sci. Bull. Lodz Univ. Tech., s. Physics, **35** (2014) 5.
[10] **Nowakowski K., Perek. A, Izdebski M., Ledzion R., Górski P.,** Sci. Bull. Lodz Univ. Tech., s. Physics, **35** (2014) 49.

WPŁYW MATERIAŁU ELEKTROD I ODLEGŁOŚCI POMIĘDZY ELEKTRODAMI NA POMIAR STAŁEJ KERRA W OLEJU RYCYNOWYM

Streszczenie

Przedstawiono wyniki badań wpływu materiału elektrody oraz odległości pomiędzy elektrodami na pomiary stałej Kerra w oleju rycynowym. Pokazano, że odległość pomiędzy elektrodami wpływa na wyniki pomiaru stałej Kerra oraz że materiał elektrod nie ma na nie wpływu.

ISSN 1505-1013